


Cost and Efficiency Requirements for Successful Electricity Storage in a Highly Renewable European Energy System

Ebbe Kyhl Gøtske^{1,2,*}, Gorm Bruun Andresen^{1,2} and Marta Victoria^{1,2,3}

¹Department of Mechanical and Production Engineering, Aarhus University, Denmark

²iCLIMATE Interdisciplinary Centre for Climate Change, Aarhus University, Denmark

³Novo Nordisk Foundation CO₂ Research Center, Aarhus University, Denmark

 (Received 9 August 2022; revised 6 April 2023; accepted 10 April 2023; published 11 May 2023)

Future highly renewable energy systems might require substantial storage deployment. At the current stage, the technology portfolio of dominant storage options is limited to pumped-hydro storage and Li-ion batteries. It is uncertain which storage design will be able to compete with these options. Considering Europe as a case study, we derive the cost and efficiency requirements of a generic storage technology, which we refer to as *storage-X*, to be deployed in the cost-optimal system. This is performed while including existing pumped-hydro facilities and accounting for the competition from stationary Li-ion batteries, flexible generation technology, and flexible demand in a highly renewable sector-coupled energy system. Based on a sample space of 724 storage configurations, we show that energy capacity cost and discharge efficiency largely determine the optimal storage deployment, in agreement with previous studies. Here, we show that charge capacity cost is also important due to its impact on renewable curtailment. A significant deployment of storage-X in a cost-optimal system requires (a) discharge efficiency of at least 95%, (b) discharge efficiency of at least 50% together with low energy capacity cost (10 €/kWh), or (c) discharge efficiency of at least 25% with very low energy capacity cost (2 €/kWh). Comparing our findings with seven emerging technologies reveals that none of them fulfill these requirements. Thermal energy storage is, however, on the verge of qualifying due to its low energy capacity cost and concurrent low charge capacity cost. Exploring the space of storage designs reveals that system cost reduction from storage-X deployment can reach 9% at its best, but this requires high round-trip efficiency ($\text{RTE} \geq 90\%$) and low charge capacity cost (35 €/kWh).

DOI: [10.1103/PRXEnergy.2.023006](https://doi.org/10.1103/PRXEnergy.2.023006)

I. INTRODUCTION

To comply with global climate commitments [1] and greenhouse gas reduction targets, a massive deployment of renewable generators, composed of wind turbines and solar panels, is anticipated [2]. The integration of variable renewable generators is associated with some challenging aspects. The variable power output necessitates backup reserves, and increased transmission capacity is required to even out production over larger areas [3]. Extensive literature exists on the variability of solar and wind power generation [4–8]. Where diurnal cycles dominate solar generation, synoptic temporal fluctuations dominate wind

generation. In Europe, both show a complementary seasonal cycle [9,10]; thus, an optimal seasonal mix of wind and solar exists [11,12].

To help relieve the aforementioned challenges, one option is to balance the fluctuations of variable renewable energy production locally in time with the implementation of electricity storage. Here, electricity storage refers to the conversion from electrical energy to a storage energy carrier that is converted back to electricity when discharged at a later time step. Similar to the temporal variability of wind and solar, different time scales apply to electricity storage. For grid stability, certain technologies perform frequency or voltage regulation, intradaily smoothing of diurnal variability, or balancing of synoptic or seasonal variation [13–15]. In this study, we limit ourselves to utility-scale electricity storage capable of providing balancing on a time frame longer than an hour.

Based on the already deployed capacity, pumped-hydro storage (PHS) constitutes the majority (> 90%) of electricity storage, globally [16,17]. In Europe, PHS has a cumulative capacity of 55-GW power capacity [18] and

*ekg@mpe.au.dk

Published by the American Physical Society under the terms of the [Creative Commons Attribution 4.0 International](https://creativecommons.org/licenses/by/4.0/) license. Further distribution of this work must maintain attribution to the author(s) and the published article's title, journal citation, and DOI.

1.3-TWh energy capacity [19]. Electrochemical batteries account for only 1% of today's storage capacity worldwide [20] (in Europe, residential batteries constituted 5.4-GWh storage capacity in 2021 [21]), but contribute to a large extent to the short-range primary responses to continuous and sudden voltage and frequency instabilities [22]. In addition, lithium-ion (Li-ion), which currently accounts for 78% of the battery systems in operation, has shown a large potential: over the last decade, Li-ion battery packs have shown learning rates of 20%, contributed substantially by the large growth in battery electric vehicles (BEVs) [23].

In the literature, power system models often use batteries to represent short-term storage and hydrogen (H₂) with electrolyzers and fuel cells as long-term storage [24,25]. In a low carbon-intense energy system, electricity storage is far from the only hydrogen use case. Hydrogen infrastructure is essential for the energy demands that are difficult to electrify, e.g., industrial processes or sections of the transport sector [26,27]. In systems with the coexistence of H₂ and Li-ion batteries, Victoria *et al.* [15] found that significant electricity storage capacities are less likely to emerge with CO₂ emission reductions lower than 80% relative to 1990 levels, in agreement with other studies [24,25,28]. Victoria *et al.* [15] and Brown *et al.* [29] showed that the presence of BEVs replaces the need for high volumes of stationary battery storage, and, in general, that flexibility introduced by sector coupling further delays the moment in CO₂ emission reduction in which large storage capacities will be needed. In addition to this, Wang *et al.* [30] showed that it is not certain that storage is always the cost-optimal strategy, compared to overplanting renewable capacities. This raises the question of under which circumstances electricity storage will be competitive.

Prior studies have evaluated the technoeconomic potential and required characteristics of electricity storage to occur in renewable power systems [14,31–35]. With the scope of guiding storage technology development, Sepulveda *et al.* [31] presented the idea of a technology design space. The design space contains combinations of storage costs and efficiencies to evaluate the potential for long-duration energy storage systems in North-American power grids. They showed that competitiveness with firm low-carbon-emitting generators highly depends on the storage energy capacity cost and discharge efficiency, whereas charge and discharge capacity costs and charge efficiency are of secondary importance. Both Sepulveda *et al.* [31] and Ziegler *et al.* [33] found a threshold of \$20/kWh energy capacity cost for the storage to become favorable to the system. Studies by Dowling *et al.* [32] and Tong *et al.* [14] both showed that low-cost energy storage has a high potential of reducing the total cost of the power system. Parzen *et al.* [35] considered the effect of including competition between multiple storage options in a European-wide power system cost-optimization model. As an evaluation metric, they used the optimal storage capacity as a

market potential indicator. Here, the optimal storage capacity refers to the deployment of a given storage technology that entails the minimum total system cost. They showed that the system value of storage integration is not only determined by the cost but also by other performance measures such as the efficiency.

The previously reported results are subject to all or some of the following methodological limitations:

- (a) They are obtained with single-node models that do not include the flow of electricity through transmission lines (i.e., copper-plate models). In that way, balancing through regional integration is neglected, and information on regional bottlenecks is lost. Moreover, regional differences within the energy mix are not accounted for, i.e., solar-wind share in every node, which also impacts the storage needed in the system.
- (b) The analyses do only consider the power system. Integrating other energy-consuming sectors such as the heating, transportation, and industry sectors has been found to change the storage requirements [15,36]. With sectoral integration, the electricity demand is substantially increased. A certain share of the additional demand from sectoral integration can be considered flexible, i.e., the production of an energy carrier can be shifted in time from the consumption. In addition, other energy-consuming sectors include other storage mechanisms, e.g., hot water tanks in the heating supply or BEV batteries that can provide additional demand flexibility. Thus, considering only the power system when determining the potential electricity storage capacity needs in a low-carbon-emitting system could lead to a substantial misestimation.
- (c) Storage investment costs and efficiencies are assumed fixed and reflect current or predicted future cost and efficiency levels. Therefore, the results obtained in the given studies are constrained by the assumptions made of each specific technology.

With PHS and batteries as dominant storage options, and the integration of flexible demand options from sector coupling, it is not clear which requirements are needed for an additional storage technology to enter the cost-optimal system. Literature has shown that, in renewable power system capacity-expansion models, low energy capacity cost and high discharge efficiency are good prerequisites. The former incentivizes an expansion of the storage to overcome long periods with renewable droughts, while the latter represents a high utilization of the stored energy with less energy loss. It is not known whether this priority is cost optimal in a sector-coupled system, and which other strategies could also apply to a qualified technology. To build upon the existing body of literature and overcome

the mentioned limitations, we raise the following research question.

- (a) Which characteristics are needed for a successful additional electricity storage technology to enter the cost-optimal system design, considering the presence of other storage options such as PHS and batteries, in a sector-coupled interconnected renewable energy system?

To help enlighten this, we use a state-of-the-art energy system capacity and dispatch optimization model to derive the space of cost-competitive electricity storage technologies, on top of PHS and battery storage. In this study, we refer to the group of additional electricity storage technologies as “storage-X” and use the term “design space” to describe the space of cost-competitive storage-X options. The derivation is computed when already accounting for the competition from other backup reserves and interconnectivity, and the integration of the heating, transportation, and industry sectors. We do not limit ourselves to fixed investment costs or efficiency assumptions. Instead, we examine the required characteristics (charge and discharge power capacity costs, charge and discharge efficiencies, energy capacity cost, and self-discharge) of a generic storage technology to feature in the system, similar to Ref. [31]. This study contributes to the existing literature by also including the effect of linking the power system with other energy-consuming sectors since this has shown a high impact on the storage needs, both in terms of volume and the characteristic [15,36]. Furthermore, we resolve the system with a network that distributes the renewable resources and consumption over the geographical domain. In this way, we also account for the regional congestion in the transmission connecting each of the regions that is an important factor in the assessment of the storage capacity allocation.

Section II presents a short review of the current state of seven emerging storage technologies that we consider as storage-X candidates. The model framework to derive the storage-X requirements to appear in the optimum system is presented in Sec. III. Our results, which cover the design requirements for storage-X and a delineation of the corresponding impact on the system design, are presented in Sec. IV. Section V encapsulates our findings in a discussion on whether current technologies can comply with the derived requirements, followed by the main conclusion of our work in Sec. VI.

The code and data used for producing the figures are openly available under an open license on Github [37].

II. CURRENT STATE OF STORAGE-X CANDIDATES

The additional utility-scale electricity storage technology appearing in a decarbonized energy system

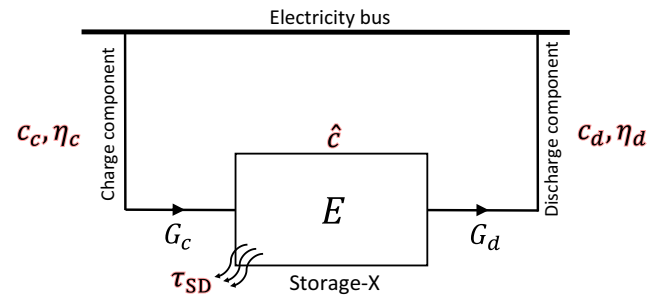


FIG. 1. Storage-X parameters. Highlighted parameters (charge and discharge power capacity costs c_c and c_d , charge and discharge efficiencies η_c and η_d , energy capacity cost \hat{c} , self-discharge time due to standing losses τ_{SD}) define the storage design, whereas the remainder (charge and discharge power capacities G_c and G_d , and energy capacity E) represent the volume of storage.

could potentially be provided by a wide range of different storage technologies. A wide palette of additional storage technologies is emerging [38]. Here, we review the current state of seven storage-X candidates, based on their proven deployment scale together with expected energy efficiency and capacity costs. Before this, we establish the parameters used for this comparison in Fig. 1. The generic storage itself is characterized by a storage energy capacity cost \hat{c} (€/kWh) and a self-discharge time τ_{SD} (days), assuming an exponential decay of the state of charge:

$$\bar{e}_t = \bar{e}_{t_0} \exp\left(-\frac{t}{24\tau_{SD}}\right). \quad (1)$$

Here, \bar{e}_t is the state of charge (SOC), i.e., the fraction of the storage energy capacity contained at time t (hours), and \bar{e}_{t_0} is the initial SOC. We use the subscript “SD” to signify the distinction from another characteristic time constant of the storage, namely, the duration (i.e., the ratio between the optimal storage energy capacity and the discharge power capacity).

The storage technology is furthermore characterized by charge and discharge power capacity costs, c_c (€/kW) and c_d (€/kW), and charge and discharge efficiencies, η_c (%) and η_d (%). Here, power capacity costs are given per unit of electricity.

The combination of the six parameters constitutes the storage configuration (i.e., the design) of storage-X. Installed energy capacity and power capacities, E , G_c , and G_d , define the volume of storage.

Here, we consider a portfolio of seven emerging storage technologies, covering both thermomechanical and chemical energy storage. For the thermomechanical storage technologies, we refer to the thorough review by Gautam *et al.* [38] from which we acquire the costs and efficiency assumptions for 2025. For the remaining technologies, we use data from Refs. [31,39–41]. The reported data are

TABLE I. Reported capacity cost, efficiency, and self-discharge time. Charge and discharge power capacity cost c_c and c_d , charge and discharge efficiency η_c and η_d , energy capacity cost \hat{c} , self-discharge time due to standing losses τ_{SD} , for seven emerging storage technologies. Values are obtained directly from or calculated based on data from Refs. [31,38,53]. See Appendix A for these calculations. If not reported, we assume zero standing loss.

| | \hat{c} (€/kWh) | c_c (€/kW) | c_d (€/kW) | η_c (%) | η_d (%) | τ_{SD} (days) |
|-------------------------------------|----------------------|-----------------|-----------------|-----------------|-----------------|-----------------------|
| TES [31,38] | 8 | 38 | 864 | 98 | 38 | 100 |
| H ₂ ^x [39–41] | 11 | 450 | 1100 | 68 | 50 | ∞ |
| MSES [38] | 17 | 104 | 1040 | 99 | 43 | 100 |
| PTES [38] | 19 | 326 | 653 | 220 | 25 | 100 |
| ACAES [38] | 26 | 314 | 629 | 92 | 65 | 100 |
| LAES [38] | 31 | 562 | 562 | 77 | 65 | 200 |
| RFB [31] | 115 | 176 | 176 | 85 | 85 | ∞ |

converted into the six descriptive storage-X parameters described above. See Appendix A for these calculations. The following subsections shortly describe the fundamental mechanisms behind every storage concept. A summary of investment costs and efficiencies is presented in Table I below.

A. Adiabatic compressed air energy storage

The adiabatic compressed air energy storage (ACAES) is a thermomechanical energy storage. In an ACAES, electrical energy is utilized to power the compression of atmospheric air to high-pressure air. Subsequently, the pressurized air is stored, either in an underground cavern or an overground pressurized tank. In the case of overground tanks, the system can be modularized, allowing the size of the plant to be scaled according to specific needs. Thermal energy generated in the compression is stored in parallel, making it an adiabatic compressed air energy storage. When discharged, the compressed air is released and heated by the thermal energy storage, to run a gas turbine which produces electricity. In that way, the heat recovery avoids the need for additional heat (usually obtained with the combustion of fossil gas) injection in a diabatic compressed air energy storage (DCAES), and it increases the overall energy round-trip efficiency of the storage system. DCAES has been proven on utility scale (a 321-MW plant in Huntorf, Germany built in 1978 [42] and a 110-MW plant in McIntosh, USA built in 1990 [43]). The first large-scale ACAES plant (100 MW and 400 MWh) was reported to have been commissioned in Zhangjiakou, China, in 2022 [44]. Prior to this, ACAES was yet to be demonstrated on a commercial scale [45].

B. Redox-flow battery

The redox-flow battery (RFB) is an electrochemical energy storage. A vanadium redox-flow battery is mentioned as the most promising of the available redox-flow batteries for large-scale energy storage [46]. The RFB is different from a Li-ion battery since it separates the electrolyte from the cell stacks in two exterior tanks. One of the tanks contains the positive electrolyte solution while the second tank contains the negative solution. The vanadium electrolyte solution flows without phase change in a circuit driven by pumps, in which the electrolyte tanks are connected to the anode (negative side) and the cathode (positive side) of the cell stack, without any mixing. Electricity is converted into chemical energy and vice versa through a reversible reduction and oxidation (redox) reaction. This conversion occurs at high efficiency (round-trip energy efficiency of 65%–80% according to Ref. [31]; Vinco *et al.* [46] reported a range of 69%–91%) compared to other energy storage technologies. Because of this design, the energy capacity is decoupled from the power capacity, which qualifies it for long-duration energy storage [47]. Recently, China commissioned a 100-MW and 400-MWh vanadium RFB to the grid in Dalian, which at the time of writing is the largest facility worldwide [48].

C. Molten-salt energy storage

Molten-salt energy storage (MSES) is a thermomechanical energy storage that stores electricity as sensible heat (i.e., temperature increase without phase change). Electrical energy is converted into heat through resistive heaters that occurs at almost 100% energy efficiency. The liquid salt is contained either in a singular tank with a thermocline or in a two-tank (hot and cold) configuration. The stored heat is converted back to electricity typically through a steam-based Rankine cycle. The discharge efficiency is thus limited by the achievable temperature of the storage. Albeit a higher investment cost compared to the single tank, the two-tank system is more common due to its better performance. The two-tank system is capable of sustaining its output temperature throughout the process of discharging. For the single tank, the output temperature decreases when the thermocline reaches the top of the tank, reducing the efficiency of the discharging stage [49]. Today, molten-salt facilities are mostly associated with concentrated solar power plants, while large-scale MSES electricity storage is yet to be demonstrated.

D. Solid thermal energy storage

Solid thermal energy storage (TES) is a thermomechanical energy storage and is in the same category as MSES. It is similarly charged with electrical resistive heaters to increase the temperature (i.e., sensible storage) of a container with stacked rock material, firebricks, or other low-cost solid material that is thermally and chemically

stable at high temperatures. The thermal energy is converted back to electricity through a Brayton cycle. Such setups are also known in the literature as Carnot batteries [50]. Here, data are acquired from Sepulveda *et al.* [31], who assumed firebricks as the storage medium. A demonstration plant exists in Germany (1.5 MW and 130 MWh) [38].

E. Pumped thermal energy storage

Pumped thermal energy storage (PTES) is a thermomechanical energy storage that utilizes the same mechanisms in a heat pump to achieve high charge efficiency. It consists of a dual tank system (one hot and one cold), each containing a packed bed of volcanic rocks. The system is charged with a heat pump cycle using air as its working fluid, which ensures a charge energy efficiency above 200%. In the charging process, air from the cold tank is compressed and transferred to the hot tank. During this stage, one tank attains a high temperature (approximately 600 °C) while the other one reaches a very low temperature (approximately -30 °C). In the discharge stage, the direction of the airflow is reversed, utilizing the high-temperature difference gained to run a Brayton cycle, generating electricity back to the grid [38]. At the time of writing, large-scale (> 1 MW) demonstrations have been projected but not yet showcased.

F. Liquefied air energy storage

Liquefied air energy storage (LAES) can also be classified as a thermomechanical energy storage. In the charging stage, electricity is utilized to power the compression of ambient air until it reaches high pressure (approximately 200 bar). The compressed gaseous air is then cooled [compression and subsequent (inter)cooling might occur over several stages], reaching cryogenic temperatures and a liquid state. The heat acquired from the cooling can be stored for the later discharge stage, increasing round-trip efficiency. When discharged, the air is exposed to atmospheric air and/or the stored heat, which entails an expansion and evaporation through a turbine generating electricity [38,51]. Large-scale plants have been demonstrated, e.g., the Pilsworth plant in the UK (5 MW) [52].

G. Hydrogen electricity storage

Hydrogen (H₂), on top of its other wide-ranging applications, can act as a power-to-power storage option. In such a case, hydrogen is produced with electricity through water electrolysis, either with alkaline or proton exchange membrane (PEM) electrolyzers. The H₂ is then stored in either underground salt caverns or overground steel tanks. At a later stage, the H₂ can be converted back to electricity through fuel cells or in a combustion turbine. Here, we assume alkaline electrolyzers [39], overground steel tanks [41], and PEM fuel cells [40]. We refer to this option as

H₂^X in which the superscript X indicates that we treat it as a storage-X technology, meaning that it can only be converted back to electricity.

The acquired data for the seven abovementioned technologies are presented in Table I, sorted according to their energy capacity costs.

Each of the configurations is mapped in the radial plot in Fig. 2. Here, the six axes represent the parameters describing storage-X. In a hypothetical case, the best-performing and most competitive storage would be characterized by zero capacity cost and 100% energy conversion efficiencies with zero standing losses. In this depiction, such an ideal storage configuration would be located in the center of the figure. Moving towards the exterior on one of the six axes is equivalent to either higher investment costs, lower energy efficiency, or higher standing losses. Here, we highlight the characteristics of a TES and a RFB. The two storage technologies have distinct characteristics indicated

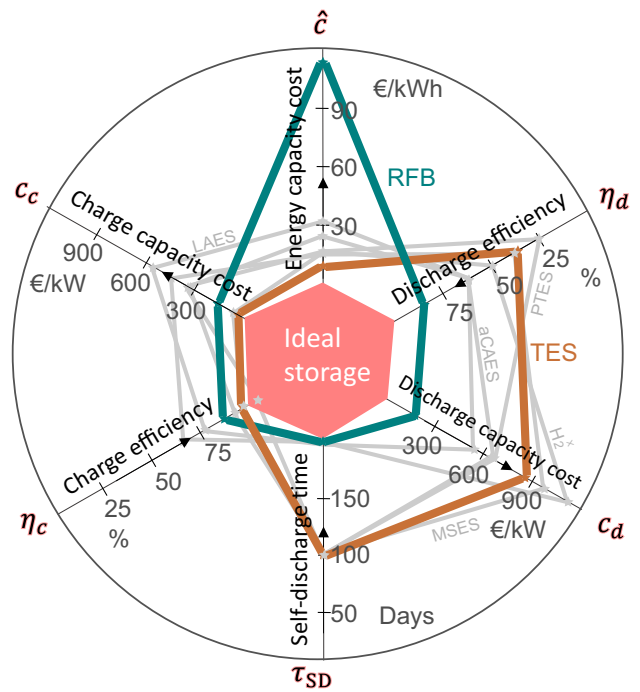


FIG. 2. Visual comparison of storage technologies. The seven storage technologies, each given by a combination of six design parameters (charge η_c and discharge η_d efficiencies, charge c_c and discharge c_d capacity costs, energy capacity cost \hat{c} , and self-discharge time τ_{SD}), are depicted. Highlighted are the thermal energy storage (TES) and redox-flow battery (RFB). On a given axis, when near the circular exterior, the technology is subject to a poor parameter (e.g., high capacity cost, low efficiency, or short self-discharge time). Oppositely, in the proximity of the center, the technology performs well on the given parameter. Because of the characteristics of TES and RFB, we see a distinct difference in the deviation from the ideal storage. Pumped-thermal energy storage (PTES) crosses the boundary of the ideal storage since the charge energy efficiency is above 1.

by the parameters deviating from the ideal storage. RFB has a pronounced high-energy capacity cost, whereas TES deviates from the ideal storage on the discharge efficiency, discharge capacity cost, and self-discharge axes.

III. METHODOLOGY

The emerging technologies presented in Table I are examples of storage designs currently being developed. It is unclear whether their parameter combinations are sufficiently favorable for the technologies to appear in the cost-optimal energy system design. To shed light on this, we follow a workflow to derive the requirements for a general storage technology to be optimally deployed, on top of batteries and PHS, in a future highly renewable energy system. For this investigation, we consider the European energy system as a case study. To determine the cost-optimal system design, we use PyPSA-Eur-Sec, which is an open energy system optimization model, described in the following subsections. The workflow behind this investigation is visualized in Fig. 3.

A. Energy system model: PyPSA-Eur-Sec

PyPSA-Eur-Sec is a linear model that performs a cost optimization subject to constraints (see Appendix B for the mathematical formulation). In essence, it finds the optimal combination of generation technologies (solar, wind, gas,

etc.), storage technologies (batteries, storage-X), and conversion technologies (heat pumps, electrolyzers) in every node to minimize the system costs while making sure that enough energy is available at all times to supply the demand (energy balance constraint). Electricity can be produced locally or imported from neighboring nodes through transmission lines, represented by the linearized power flow model assuming lossless links [54]. The variables that are optimized include the capacities (of different generating, storage, and conversion technologies) and how they are operated at every time step. Besides ensuring that the energy balance is fulfilled for every node and at all times, the optimization includes other constraints that, e.g., limit the maximum global CO₂ emissions. The model measures the direct CO₂ emissions from electricity and heating production, industrial processes, and combustion of fossil oil, e.g., for internal-combustion engines in land transport. The model does not represent the full CO₂ footprint of each asset but only considers emissions throughout their operation.

In this study, the model is resolved with a network of 37 nodes spanning 33 countries (see Fig. 4), all members of the European Network of Transmission System Operators for Electricity (ENTSO-E). Distribution grid investment cost is included but the distributional network is not modeled since we only focus on storage capacity allocation in the high-voltage grid. The optimization is computed for

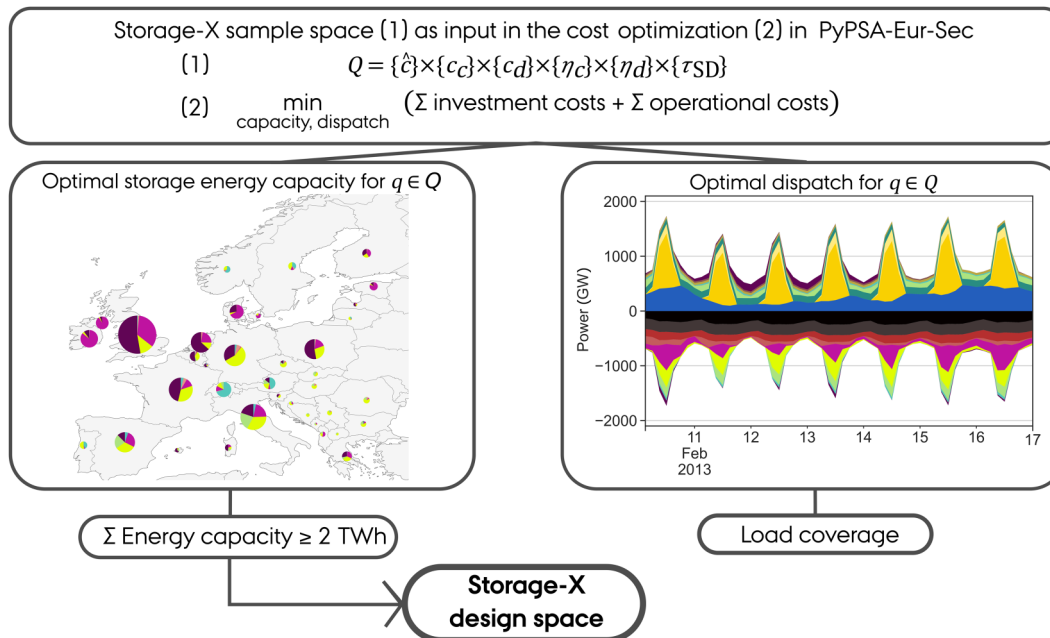


FIG. 3. Method workflow. Storage-X sample space is used as input in the energy system model PyPSA-Eur-Sec to run as many scenarios as the size of the sample space. The capacity and dispatch are optimized in each of the scenarios. Subsequently, the storage-X deployment is evaluated based on the optimal energy capacity. If it fulfills a total energy capacity of ≥ 2 TWh, the given configuration qualifies for the storage-X design space. The load coverage (LC) is obtained from the dispatch as a proxy for the level of storage contribution to balance the electricity load and supply. The LC metric is used to compare the configurations but is not used as a selection criterion for the derivation of the design space.

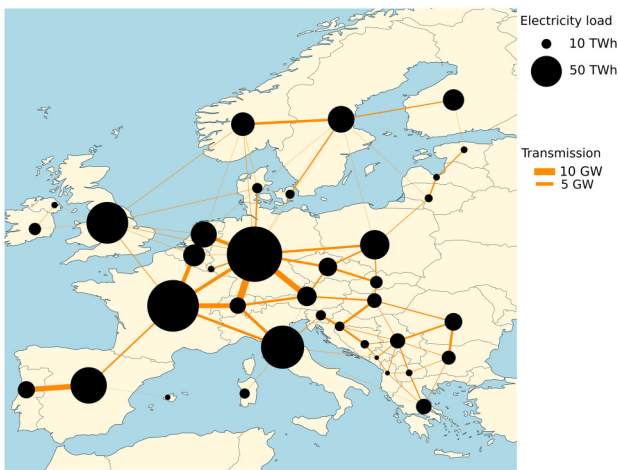


FIG. 4. Network topology. The network consists of 37 nodes distributed over 33 European countries, all members of ENTSO-E. Italy, Spain, Great Britain, and Denmark have multiple nodes since the countries cover different synchronous regions. The size of the nodes corresponds to the historical annual electricity consumption for 2013. The nodes are interconnected with ac and dc high-voltage lines corresponding to today's capacity including transmission lines projected in the TYNDP 2018 by ENTSO-E [55].

one year with a 3-hourly resolution. For this reason, only storage with duration (i.e., energy-to-power ratio) larger than or equal to 3 h is considered for the capacity expansion since fluctuations within each time step are implicitly smoothed by the averaging. The internodal transmission capacity is exogenously included in the model and equals current transmission lines with the addition of lines under construction expected to be commissioned according to the ten-year network development plan (TYNDP 2018) by ENTSO-E [55]. For clarity, we refer the reader to Tables S1 and S2 within the Supplemental Material [56] for the capacities of the included ac and dc interconnections, respectively.

The model assumes an ideal market with perfect competition between all included technologies and long-term market equilibrium, i.e., energy technology recovers exactly its full costs. Furthermore, the model assumes perfect foresight of energy supply and demand. This implies that the resources are distributed optimally over the year based on the year-ahead informed weather conditions and consumption patterns. For such a reason, any storage acting as a security backup against unforeseen energy droughts is not included. All technology costs and lifetime estimates are reported in Ref. [57]. Here, technology costs are acquired for 2030 to account for expected technology cost reduction, while selecting a year relatively close to the present to reduce uncertainty in cost estimations. The investment costs are annualized with the reported lifetime estimates of each asset, assuming a discount rate of 7%.

The electricity load prior to optimization reflects historical national consumptions reported by ENTSO-E, collected from Open Power System Data [58]. This is based on 2013 and the data include the electricity demand in the industry. The electricity load is assumed price inelastic, which means that we do not include any demand response on the marginal electricity price. An additional electricity demand arises when including the heating and transport sectors while enforcing a CO₂ emission limit. The CO₂ emission limit causes a fraction of the heating demand to be electrified with the inclusion of heat pumps or resistive heaters, while the remainder can be covered by combined heat and power (CHP) plants or gas boilers. Land transport is included exogenously. Here, we assume that 85% of the demand for land transport is delivered from BEVs, while the remaining 15% is covered by hydrogen fuel cell vehicles. The latter represent transport difficult to electrify such as heavy construction machinery or long-haul trucks for which a higher gravimetric energy density is more suitable. The industry sector includes the energy demand, e.g., for steel, iron, and aluminum production, as well as the production of chemicals such as ammonia and methanol, and the CO₂-intense cement production. The methane feed-in for some processes can be either fossil based or synthetic, decided by the optimization. For other processes, carbon capture can be deployed, if cost optimal. In addition, the model also includes energy demands in aviation (kerosene from synthetic or fossil oil) and shipping (H₂ and oil), as well as a European biomass supply (both solid and gaseous). For fuel production from synthetic and renewable gases, e.g., green hydrogen production with electrolyzers, additional power generation capacity is needed, compared to an electricity-only system. Figure 5 depicts a simplified scheme of how the generators, links, and storage are connected in the model. Each bus may have multiple loads and may be interlinked with multiple other buses that the presented schematic does not include for simplicity. For a detailed description of the sector representation, we refer the reader to Ref. [2].

Here, we consider a future European energy system that is on the verge of achieving net-zero emissions. The annual net CO₂ emissions of the considered system are restricted to 5% of the 1990 levels. Gross emissions can exceed this limit if they are compensated by negative-emission technologies (direct air capture or carbon capture on point sources) that are deployed if cost optimal. The optimization is performed *overnight*, which means that we consider one calendar year for the capacity deployment and energy dispatch without accounting for the pathway from today's system toward the resulting system. We investigate three system compositions (SCs).

SC1. **Electricity:** The electricity demand is fixed to the historical levels while transforming the electricity supply to comply with the CO₂ emission constraint,

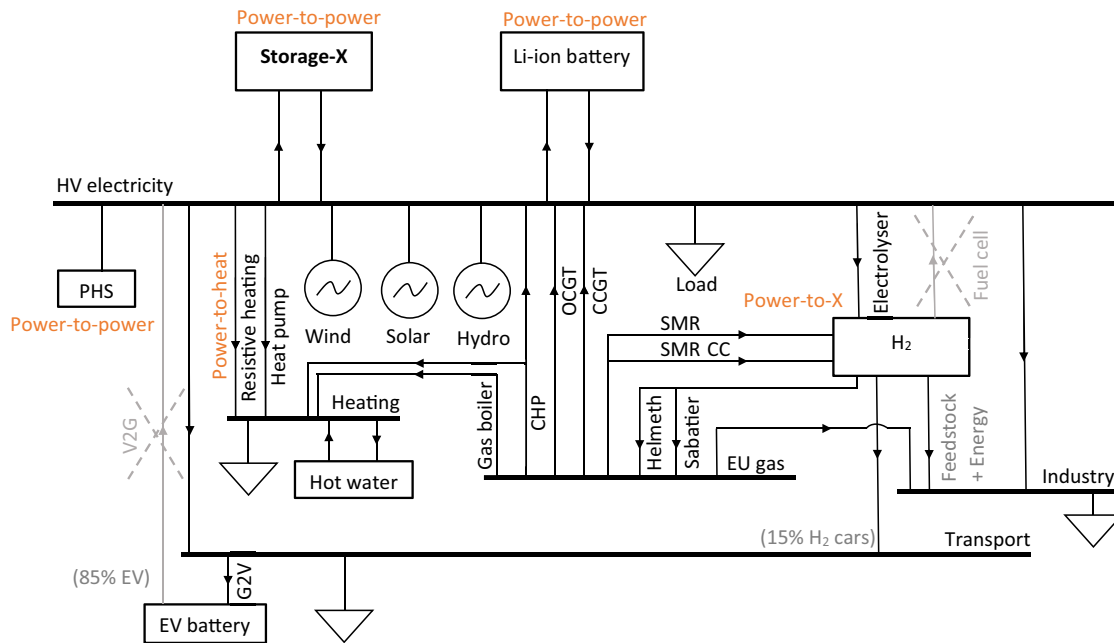


FIG. 5. Schematics of storage-X integration in the fully sector-coupled energy system. Storage-X is linked to the high-voltage (HV) electricity bus. Hydrogen is only used as a power-to-X technology and, thus, does not have a direct link back to the HV electricity bus. Such a setup (power-H₂-power) is intendedly resembled by storage-X. Furthermore, smart charging, here named grid-to-vehicle (G2V), is included when adding land transport, allowing flexible charging of the EV batteries. Vehicle-to-grid (V2G), i.e., EV battery supplying power to the high-voltage electricity bus, is not allowed. In the fully sector-coupled system, solid biomass and biogas usage is also allowed, which is not depicted in the diagram for simplicity.

without the inclusion of other energy-consuming sectors.

SC2. **Electricity + heating + land transport:** In addition to transforming the electricity supply, the system includes the heating sector and the energy consumption in the land transport sector.

SC3. **Fully sector coupled:** The system includes the energy consumption in the heating, land transportation, and industry (including feedstock, aviation, and shipping) sectors, and the supply of biomass.

TABLE II. Model assumptions in this study. Temporal and spatial resolutions, technology cost assumption year, transmission volume level, and the net CO₂ emission constraint used in the three system compositions (SC1–SC3).

| Assumption | |
|-------------------------------|--|
| Type | Overnight optimization |
| Time resolution | 3 h |
| Network resolution | 37 nodes |
| Weather year | 2013 |
| Technology costs | 2030 |
| Transmission | Fixed to today + TYNDP |
| Net CO ₂ emissions | 5% relative to 1990 SC1: 74.1 MtCO ₂ SC2: 148.2 MtCO ₂ SC3: 229.9 MtCO ₂ |

The main model assumptions specific to this study are summarized in Table II.

B. Generators

The renewable generators available to the system are wind (off- and onshore), solar PV (utility and rooftop), and hydropower (reservoir and run-of-the-river). We distinguish between two voltage levels in the grid: high voltage (transmission grid) and low voltage (distribution grid). The renewable generators are connected to the high-voltage grid, except the solar rooftop, which is attached at low voltage. For wind and solar, the installable capacity is limited by the estimated potentials based on the available land use from the Corine Land Cover database [59] subtracting Natura 2000 protected areas [60]. The following limits are imposed, based on the study by Victoria *et al.* [2]: on- and offshore wind are limited to 20% of available land, utility-scale solar PV is limited to 9%, whereas the rooftop PV potential is estimated according to the population density. Hydropower generation capacities, comprised run-of-the-river and reservoir, are included exogenously since most of the potential is assumed to be exploited, and kept fixed at today's capacity (34.5 GW for run-of-the-river and 99.6 GW for reservoir) [61]. Time series of hydro inflow as well as wind and solar capacity factors are obtained with ATLITE [62] and ERA5 [63], using weather data for 2013.

In every 3-h time step, wind turbines and solar panels can provide electricity to the grid proportional to the concurrent capacity factor. In the case of exceeding the demand and/or congestion in the transmission, the excess energy is curtailed. The curtailed energy in each time step is calculated as

$$\text{Curtailed energy}_t(\%) = \frac{\sum_{n,s} (\bar{g}_{n,s,t} G_{n,s} - g_{n,s,t})}{\sum_{n,s} \bar{g}_{n,s,t} G_{n,s}}, \quad (2)$$

where $\bar{g}_{n,s,t}$ is the capacity factor at time t of a variable renewable generator s , $G_{n,s,t}$ is the installed power capacity, and $g_{n,s,t}$ is the actual electricity generation.

Open-cycle gas turbine (OCGT), combined cycle gas turbine (CCGT), nuclear, and coal power plants can be deployed if cost optimal. Furthermore, in SC2 and SC3, the system can deploy CHP plants fueled with gas or biomass. Biomass and gas-fired CHP plants have the option of installing carbon capture at an additional investment and operational cost. Investment and operation and maintenance cost predictions and lifetime estimates acquired from Refs. [40,64] of the power generation technologies subject to optimization are presented in Table S3 within the Supplemental Material [56]. Capacities and locations of hydropower generation and pumped-hydro storage units that are not optimized, but included exogenously, are acquired from Powerplantmatching v0.5.3 [61].

C. Hydrogen

H₂ can be produced with water electrolysis powered by electricity from the high-voltage grid. Furthermore, it can be produced from steam-methane reforming (SMR) with or without carbon capture (CC), corresponding to blue and gray H₂, respectively. The H₂ network is installed if cost optimal. Lastly, H₂ can be converted into methane through the Helmeth or Sabatier reactions. We disallow H₂ in the model to dispatch directly as electricity back into high-voltage (HV) electricity (i.e., fuel cells are omitted) since we want to decouple the hydrogen production as part of a *power-to-X* strategy and hydrogen storage used for grid balancing. A hydrogen storage disconnected from any other bus than the HV bus, charged with electrolyzers and discharged with fuel cells, is in this study represented by storage-X. In addition, a previous study with sector coupling suggests that only a minor fuel cell capacity for grid balancing is deployed (approximately 2-GW European aggregate) in a sector-coupled European energy system [65].

D. Storage

Storage can be deployed in every node of the network. Existing PHS is included in the model before optimization, whereas the capacity of stationary Li-ion batteries and storage-X is optimized. We do not include the

TABLE III. Technology cost and efficiency assumptions for PHS. Assumptions are obtained from Ref. [67].

| Parameters | PHS |
|-----------------------|-----------|
| Investment cost | 2208 €/kW |
| Lifetime | 80 years |
| FOM | 1.0% |
| Round-trip efficiency | 75% |
| Total energy capacity | 1.4 TWh |
| Total power capacity | 56 GW |

existing storage infrastructure that solely operates within other markets than the balancing, e.g., primary frequency response. Besides electricity storage, the model can select hot-water tanks and H₂ storage to be deployed as well, to shift the production from the heating and H₂ consumption in time. EV batteries with smart charging are included when coupling with the land transport sector and act as a flexible demand.

1. Pumped-hydro storage

Existing PHS in Europe constitutes approximately 55-GW power capacity [18] and 1.3-TWh energy capacity [19]. Gimeno-Gutierrez and Lacal-Arategui [66] identified a technical potential for new PHS projects in Europe, including social and environmental constraints, but here we assume the cost-optimal potential to be fully exploited. Thus, PHS is added exogenously to the model, keeping it fixed at today's capacity. Using plant-specific data from Powerplantmatching v0.5.3 [61], this aggregates to 56-GW power capacity, and using discharge times from Geth *et al.* [19], this corresponds to 1.4-TWh energy capacity. Table III summarizes the PHS specifications used in our calculation.

2. Stationary battery storage

Battery storage in the high-voltage grid is included in the objective of the optimization problem, where energy and power capacities are subject to independent optimization. The cost and performance assumptions reflect data from the Danish Energy Agency [53] on utility-scale Li-ion batteries.

TABLE IV. Technology assumptions for battery storage. Estimates are for the year 2030, acquired from Refs. [53,68].

| Storage | Investment cost | Lifetime (years) | FOM (%) |
|-------------------------|-----------------|------------------|---------|
| Utility | 142 €/kWh | 25 | 0 |
| - Inverter ^a | 160 €/kW | 10 | 0.34 |
| Residential | 202.9 €/kWh | 25 | 0 |
| - Inverter ^a | 228.06 €/kW | 10 | 0.34 |

^aBidirectional. Battery round-trip efficiency $\eta = 96\%$.

TABLE V. Storage-X parameter sets. Cost, efficiency, and self-discharge for a fixed storage configuration (first column) and the sample space (second column).

| Parameter | Fixed | Sets |
|-------------|-----------------------|---|
| \hat{c} | 3 €/kWh | {1, 2 ^a , 5, 10 ^b , 20, 30, 40} |
| c_c | 350 €/kW _e | {35, 350, 490, 700} |
| η_c | 50% | {25, 50, 95} |
| c_d | 350 €/kW _e | {35, 350, 490, 700} |
| η_d | 50% | {25, 50, 95} |
| τ_{SD} | 30 days | {10, 30} |

^a2030 cost of underground cavern H₂ storage [53].

^b2030 cost of H₂ storage tank [53].

Residential batteries are also subject to optimization and included in the low-voltage grid, with cost assumptions from Ram *et al.* [68]. Assumed investment and fixed operation and maintenance (FOM) costs in 2030 are presented in Table IV.

3. EV Battery

For a total fleet of 217 million BEVs (corresponding to 85% of the total number of cars according to the Joint Research Centre [69]), assuming 50-kWh batteries with 11-kW chargers, this represents a cumulative EV battery storage of 5.44-TWh energy capacity and 2.39-TW charge power capacity. We assume that 50% of the fleet is available for demand side management with smart chargers, i.e., the BEV can charge when it is best for the system. The charging pattern is then subject to the optimization. The BEV battery's SOC is constrained to a minimum of 75% at 7 a.m. so that BEVs are ready for typical commuting. Dispatching electricity back to the HV electricity bus, i.e., vehicle-to-grid (V2G), is not allowed in this study, resembling a lack of user willingness to participate due to a reduced battery lifetime [70].

4. Storage-X

Similar to the study by Sepulveda *et al.* [31], we enclose all feasible combinations into a design space of successful storage configurations. Here, we classify storage as successful if it is able to play a substantial role in the decarbonized energy system. To do so, we represent each of the six storage-X parameters with a discrete range (shown in Table V) and confine all combinations in a sample space Q , here defined as the Cartesian product of all parameter sets:

$$Q = \{\hat{c}\} \times \{c_c\} \times \{c_d\} \times \{\eta_c\} \times \{\eta_d\} \times \{\tau_{SD}\}. \quad (3)$$

Every configuration within the sample space represented with sample $q \in Q$ is used as an input to calculate the optimum capacity and dispatch of the European energy system for the three system compositions (electricity (SC1),

electricity + heating + land transport (SC2), fully sector coupled (SC3)). For every q , we assume a FOM cost of 1% of investment cost for the storage and 2% for charge and discharge components, equivalent to assumptions for a H₂ electricity storage in Ref. [53]. Moreover, every configuration q has a lifetime of 30 years. Similar to other technologies, a financial discount rate of 7% is used in the annualization of the capital cost.

As proxies for the potential of every q , we calculate the Europe-aggregate energy capacity E ,

$$E = \sum_{n=1}^{37} \eta_d E_n, \quad (4)$$

and the load coverage

$$LC = \frac{\sum_{n,t} |\Delta e_{n,t}^-|}{\sum_{n,t} I_{n,t}}, \quad (5)$$

where E_n is the nodal energy capacity of storage-X, $I_{n,t}$ is the electricity load, and $|\Delta e_{n,t}^-|$ is electricity dispatched from storage-X in node n at time t . The energy capacity E_n is the maximum storable content in a considered storage in node n in units of energy before discharging. The configuration space contains different discharge efficiencies, and to account for this, the optimal aggregated energy capacity E is converted into units of dispatchable electricity by multiplying with the discharge efficiency η_d . We use the energy capacity as a metric to represent the storage market potential, similar to what was done in Ref. [35]. Here, we also use the load coverage, equal to the amount of electricity dispatched by the storage normalized with the total load, to indicate the potential contribution to covering power imbalances. Here, the total load accounts for the base load (national electricity load, including demand from the industry) and the additional load from sector coupling (e.g., the electrified heating supply, BEVs in land transport, the large H₂ production needed in a decarbonized sector-coupled energy system, etc.).

Additional balancing from backup capacities has been shown to reduce substantially when an ideal storage (i.e., 100% round-trip energy efficiency) with an energy capacity equivalent to 6 times the average hourly load is deployed in the system [71]. This corresponds to approximately 2-TWh energy capacity for the European system prior to the inclusion of electricity demand for heating and land transport. Furthermore, 2-TWh energy capacity compares well with the average European storage requirement in the two ENTSO-E 2040 scenarios, *distributed generation* (1.348 TWh) and *sustainable transition* (2.518 TWh) [72]. To encapsulate all successful storage configurations, we define, subsequent to the optimization, a lower threshold of $E \geq 2$ TWh that the storage needs to fulfill. This is evaluated for all configurations within the sample space.

The configurations from the sample space fulfilling this condition are collected and constitute the storage-X design space. The design space is the subset of the parameter values listed in Table V, where the system finds a substantial deployment of storage-X, more precisely, an energy capacity of at least 2 TWh.

To reduce computation time, when repeating the calculations for the same sample space Q in the three system compositions, we introduce a filter M that omits the samples of which the ratio of capacity cost and efficiency leads to an insignificant capacity deployment in the first round of computations in SC1. With this approach, the uniform sample space Q containing 2016 configurations is reduced to 724 configurations (see Appendix C).

E. Relative parameter importance

To compare the relative importance of the parameters determining the optimal storage-X deployment, we perform a multivariable (ordinary least squares) regression subsequent to the optimization. Here, a log-linear model $\log \hat{E}$ is used to relate the optimal energy capacity E (the response variable) to the storage parameters x (the features):

$$\log \hat{E} = \beta_0 + \sum_{k=1}^6 \beta_k \bar{x}_k \quad (6)$$

with the vector β containing the regression coefficients for the six parameters. The energy capacity is log transformed with the natural logarithm to linearize the response. Since the parameters x differ in range and units, we normalize them using a min-max scaling:

$$\bar{x} = \frac{x - \min(x)}{\max(x) - \min(x)}. \quad (7)$$

Likewise, a min-max scaling is applied to the log-transformed response variable. Following the regression, the coefficients are normalized:

$$|\bar{\beta}| = \frac{\beta}{\max(\beta)}; \quad (8)$$

thus, $|\bar{\beta}| = 1$ indicates the highest relative importance.

The regression is validated based on the adjusted R^2 . An additional measure of parameter importance ΔR_k^2 of parameter k is calculated based on a decomposition of the adjusted R^2 :

$$\Delta R_k^2 = R_Z^2 - R_{k \notin Z}^2. \quad (9)$$

Here, Z indicates the full set of parameters and $k \notin Z$ indicates the set of parameters omitting parameter x_k in the regression. A large value of ΔR_k^2 indicates that parameter x_k explains a high share of the variance of the output (optimal energy capacity).

IV. RESULTS—STORAGE-X

In the following subsections, the storage-X capacity deployment in the cost-optimal system layout is analyzed as a function of the parameters listed in Table V. Furthermore, we evaluate requirements on the cost and efficiency of storage-X to contribute significantly to the system layout, while competing with other more mature storage, backup, or flexibility options. The results are obtained for three system compositions: “electricity” (SC1), “electricity + heating + land transport” (SC2), and “fully sector coupled” (SC3).

A. Implications of sector coupling

To gain insight into the differences in system compositions and their implications for storage-X deployment, we analyze how the same period with low renewable production, signified by a drop in wind resources, is balanced in two different systems. Specifically, Fig. 6 compares the purely electricity-supply system (SC1) with the fully sector-coupled system (SC3). The results are obtained using the “fixed” storage-X configuration (Table V), with the discharge efficiency adjusted to 95%. In SC1, the system response to the wind scarcity is to discharge storage-X together with PHS and to activate the fossil-fueled OCGT. In addition, CCGT is used to cover imbalances over a longer period. In SC3, the main mechanisms to compensate for the drop in wind production are to discharge storage-X and to reduce the production of H_2 . The difference in the balancing mix between the two systems can be explained by how the CO_2 emissions are distributed. The model does not impose sector-specific CO_2 emission constraints, but instead, a global CO_2 emission constraint, and the model then determines how to distribute the emissions across the sectors. The two systems, albeit with the same CO_2 emission constraint, distribute the emissions differently. In SC1, all of the allowed CO_2 emissions (5% of 1990 levels) are allocated in the electricity supply to run fossil-fueled power plants in times of renewable droughts. When connecting with other sectors (SC2 and SC3), a large share of the emission cap is moved to other CO_2 sources that are more difficult to fully decarbonize (e.g., cement and steel production in the industrial sector,) which consequently disallows a large share of the emissions in the electricity supply. Because of this, the model chooses fossil-fueled backup capacities in SC1, but not necessarily in SC2. For this reason, the sector-coupled systems in this study may require a higher volume of storage-X, despite the new flexibility options enabled by sector coupling.

To further investigate the impact of sector coupling, we examine how the system responds to different levels of CO_2 emission constraints. We use the “fixed” storage-X configuration and conduct simulations by gradually reducing the CO_2 emissions from 10% of the 1990 levels to 0%. When more stringent CO_2 emission constraints

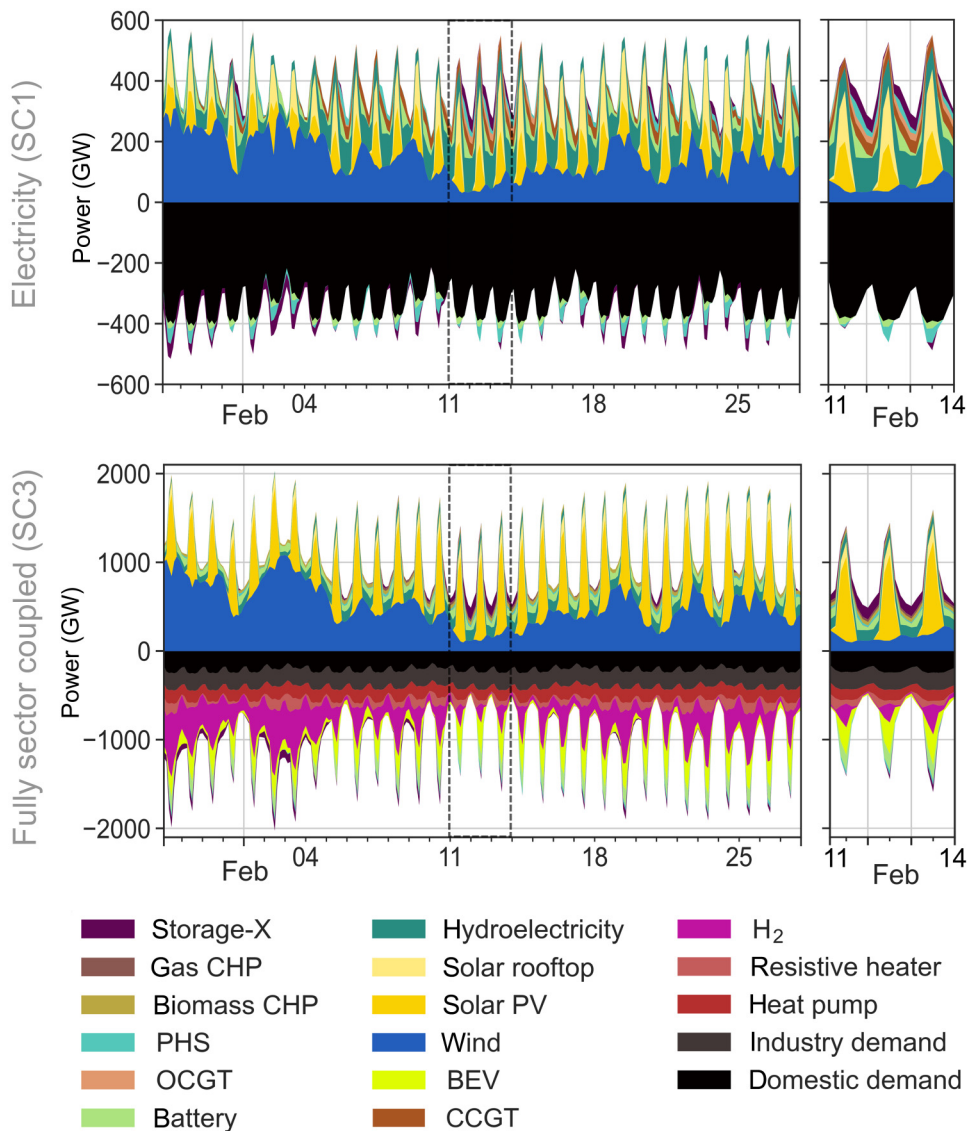


FIG. 6. Different mechanisms to balance renewable droughts. Europe-aggregate energy balance in a period with low wind production for the electricity system (top) and the fully sector-coupled system (bottom). The results are obtained with the inclusion of the “fixed” storage-X configuration (Table V) but with the discharge efficiency altered to 95%. The figure indicates a renewable drought in which storage-X is discharged from the 11th to the 14th of February caused by low wind production. Note that the y -axis range is different for the subfigures. See Fig. S1 within the Supplemental Material [56] for a representation of the full year.

are imposed, the storage-X capacity deployment in SC1 exceeds that of the sector-coupled systems (see Fig. S2b within the Supplemental Material [56]). Upon achieving net-zero emissions, the storage energy capacity in SC1 reaches 12 TWh for the fixed storage configuration. In contrast, the impact on storage energy capacity in the sector-coupled systems is less noticeable since their electricity supply is already almost fully decarbonized. For the fixed storage configuration, storage energy capacities in SC2 and SC3 reach 300 GWh at net-zero emissions.

B. Single parametric sweep

Here, we consider the case in which one parameter is altered at a time while keeping the remainder fixed according to Table V. Figure 7 depicts the resulting energy capacity deployment (top panel) and load coverage (bottom panel), used as proxies for storage potential, as a

function of the six storage-X parameters. The single-parametric sweep is performed for all three system compositions. As discussed, for all parametric ranges, the sector-coupled systems entail larger energy capacity deployment of storage-X. Concurrently, due to the increased electricity demand, the relative contribution to meeting the load, i.e., the load coverage, is reduced. The output shows different responses between the system compositions due to differences in the scaling of the electricity supply. This is consistent for all parameter levels.

For the parameter alterations, we see a consistent response for all three system compositions: an improved discharge efficiency, as well as a reduction in the charge capacity cost, reveals the highest increase in both energy capacity deployment and load coverage, over the full parameter range. Conversely, storage self-discharge due to standing losses shows a minor impact. It is, however, noticeable for SC1 that to obtain a nonzero load

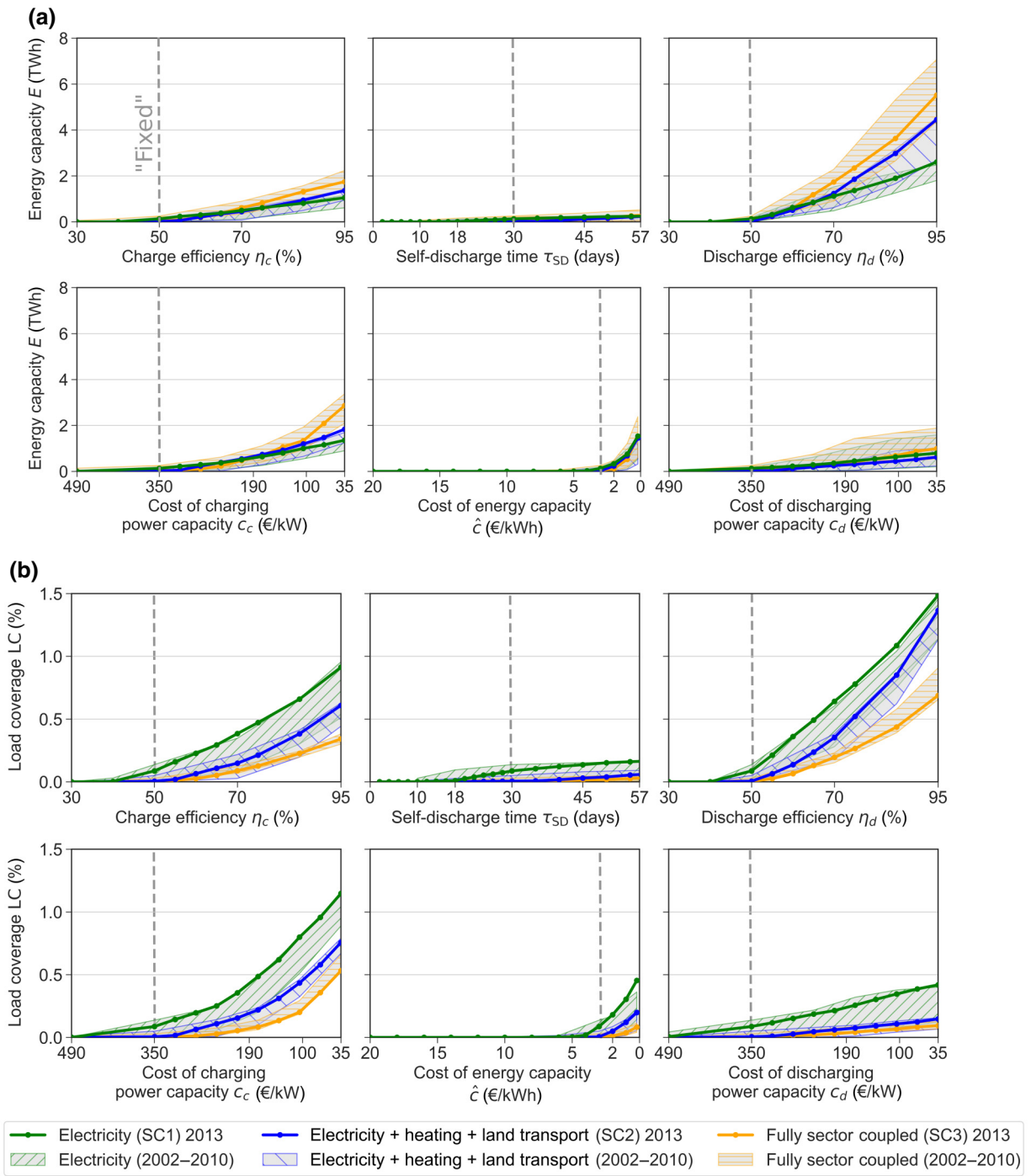


FIG. 7. Europe-aggregate (a) energy capacity, Eq. (4), and (b) load coverage, Eq. (5), of storage-X in the cost-optimal system design. Results are obtained by varying one storage-X parameter at a time for the 2013-weather year (solid lines) while keeping the remaining parameters fixed according to the “fixed” configuration (Table V). This is repeated for an interval of different weather years from 2002 to 2010 (hatched area). The energy capacity is in units of dispatchable electricity. Comparisons with existing PHS and optimized battery capacities are shown in Figs. S3–S5 within the Supplemental Material [56].

coverage, the self-discharge time needs to be above 18 days (10 days when examining other weather years). The negligible gain of having low standing losses can be explained by storage-X not being used by the model as

seasonal storage. Intermediate parameters, i.e., the parameters that cause a higher response than the self-discharge time but a lower response than the discharge efficiency and charge capacity cost, are the charge efficiency, energy

capacity cost, and discharge power capacity cost. Noteworthy is the response to reducing energy capacity cost that is negligible until reaching ≤ 5 €/kWh. Below this limit, the parameter improvement leads to a noticeable increase in energy capacity within a small domain, i.e., the response curve is subject to a steep slope, which explains why previous studies find this, together with discharge efficiency, to be the most determining parameter.

The choice of weather year has been shown to impact the optimal storage capacity deployment in the literature [73]. To address this, we first perform a sweep across the years with the fixed storage-X configuration (defined in Table V) from 1997 to 2012 and compare this with the results obtained for 2013. Here, in accordance with the literature, we observe a high sensitivity on the optimal storage energy capacity to the considered weather year (see Fig. S2a within the Supplemental Material [56]). The impact of weather input is however not consistent across the three system compositions. For SC1, the maximum storage-X deployment occurs using 2010 weather data, while for SC2, the same year leads to a minimum deployment. To account for this sensitivity, we include additional weather years in the single-parametric sweep to compare with the results obtained to the reference year (2013). The years (2002, 2003, 2006, 2008, 2010) are picked based on their distinct impact on the optimal energy storage capacity. These results are added to Fig. 7 (hatched areas). We see that, despite a considerable sensitivity to the weather year, the parametric sensitivity is stronger; thus, the observations made for one weather year still hold.

Enhancing the design of storage-X not only increases its capacity build-out, but also affects the deployment of other storage options due to competition. This is illustrated in Figs. S3–S5 within the Supplemental Material [56], which compare the capacities of the available electricity storage in the three systems. Here, stationary battery capacity is the only electricity storage competitor to storage-X since PHS capacity is fixed. The reduction in battery power capacity is particularly noticeable when improving the discharge efficiency of storage-X. At the highest level of storage-X discharge efficiency improvement (from 30% to 95%), the battery power capacity is reduced by 64% in SC1 (27% and 23% in SC2 and SC3). We conclude that a storage with a high discharge efficiency has the highest competitiveness with Li-ion batteries.

C. Design space of storage-X

The single-parametric sweep indicates a sensitivity of the resulting storage energy capacity and load coverage to individual storage parameter adjustments. As the results are based on specific values of five fixed parameters from Table V, changing these parameters could lead to different indications. In order to generalize our findings, we run a multiparametric sweep based on the predefined sample

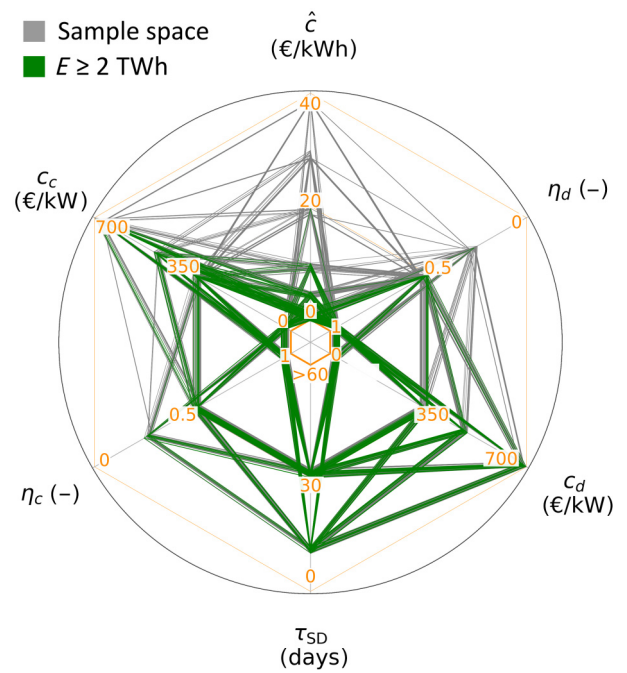


FIG. 8. Configurations fulfilling ≥ 2 TWh for the electricity system (SC1). Sample space (gray) and the derived design space (green) containing the configurations entailing $E \geq 2$ TWh. See Fig. S6 within the Supplemental Material [56] for the same depiction of the sector-coupled system, and Fig. S7 therein for the frequency of each parameter level within the design space.

space of 724 storage configurations, as described in Sec. III D 4. With the requirement of $E \geq 2$ TWh, we show how the sample space is reduced to the resulting design space in Fig. 8. The figure depicts the initial configurations of the sample space and the 205 configurations that qualify for the design space in SC1 (for depictions of SC2 and SC3, see Fig. S6 within the Supplemental Material [56]). A key selection criterion is a low energy capacity cost as the number of combinations in the design space dramatically drops when increasing the level of this parameter. Only a few combinations are present at an energy capacity cost of 20 €/kWh. A similar observation can be made for the discharge efficiency, which shows only a few combinations at 25%. The remaining axes do not, in this depiction, indicate similar limitations. The same finding is made for the sector-coupled systems, but in that case, a higher energy capacity cost is allowed (configurations are observed with 30 €/kWh for SC2 and 40 €/kWh for SC3), inviting a higher number of configurations to enter the design space.

From the linear regression [Eq. (6)], the variation of the optimal capacity deployment can also to a large extent be explained by the energy capacity cost and the discharge efficiency. This is indicated in Table VI by the normalized regression coefficients and the increase in R^2 [shown in percentage points (pps)] by adding a parameter as a descriptor to the regression. The largest coefficients are

TABLE VI. Relative importance of storage-X parameters estimated by normalized regression coefficients. The table shows the normalized coefficients from the linear regression model [Eq. (6)] of the optimal storage energy capacity of 724 storage samples. Prior to the regression, the parameters are scaled to range from 0 to 1 (min-max scaling) and the response variable is transformed with a natural logarithmic. The regression shows an adjusted R^2 of 74.6%, 74.5%, and 76.7% for SC1, SC2, and SC3, and all coefficients are significant ($p < 0.05$). The gray annotations show the increase in percentage points of the adjusted R^2 by adding the parameter to the fit, ΔR_k^2 . The color bands highlight the parameters with the highest coefficients and ΔR_k^2 .

| | | | | | | |
|------|-------------------|-------------------|------------------|-------------------|-------------------|------------------|
| SC1- | 1.0 +30.5 pps | 0.58 +16.0 pps | 0.25 +3.0 pps | 0.41 +8.5 pps | 0.85 +36.1 pps | 0.07 +0.3 pps |
| SC2- | 0.99 +25.1 | 0.59 +13.7 pps | 0.42 +7.4 pps | 0.47 +9.6 pps | 1.0 +42.4 pps | 0.16 +1.8 pps |
| SC3- | 0.93 +24.4 pps | 0.54 +10.5 pps | 0.38 +6.3 pps | 0.49 +11.4 pps | 1.0 +45.9 pps | 0.15 +1.6 pps |
| | \hat{c} | c_c | c_d | η_c | η_d | τ_{SD} |

observed for the energy capacity cost \hat{c} and discharge efficiency η_d across all system compositions. They furthermore lead to the largest increase in the adjusted R^2 . Thus, the regression suggests that the highest relative importance is within these two parameters. Following \hat{c} and η_d , the third largest coefficients are observed for the charge capacity cost c_c .

By evaluating the output of the optimization for all combinations of \hat{c} and η_d , we can identify critical parameter values that a generic storage technology is required to fulfill. These values determine the border of the optimal storage-X design space. We can divide the parameter requirements in two: (1) unconditioned requirements that are true in all cases of the considered parameter space, and (2) conditioned requirements that depend on further conditions besides the \hat{c} and η_d (e.g., power capacity costs < 700 €/kW and efficiencies $> 25\%$). Figure 9 presents the combinations of \hat{c} and η_d , and evaluates them based on whether $E \geq 2$ TWh is satisfied. The color represents the share of configurations within the sample space at the particular combination that satisfies this condition. The white annotations indicate conditioned requirements for the remaining parameters (c_d , c_c , and η_c) at a given combination. Here, τ_{SD} is not shown due to its low impact. One obvious option to maintain a high share of qualified configurations, according to the figure, is to select a high discharge efficiency and a low energy capacity cost; at such a combination, no noticeable reduction (i.e., the exclusion of configurations not satisfying the qualification condition) is observed. In that case, storage is deployed in the cost-optimal system independent of the other cost

and efficiency parameters. This is in alignment with the indications in Table VI. When deviating from the best combination in either direction of the chart, the share of qualifying configurations drops. If the deviation is too large, the share drops to 0 (indicated by the hatched area); thus, the combination disqualifies from entering the optimal design space. We use the point at which the storage parameters just meet the minimum requirements for deployment (qualification border) to describe the necessary storage parameter values. Figure 9 depicts three qualification borders, each corresponding to a certain discharge efficiency level. If the storage is attributed with a high discharge efficiency ($\eta_d = 95\%$), the qualification border (a) is located at the far right on the primary axis. This means that the full range of the energy capacity cost \hat{c} can satisfy $E \geq 2$ TWh when discharge efficiency is high, although the share of qualified configurations drops noticeably when $\hat{c} \geq 20$ €/kWh. However, when $\hat{c} \geq 20$ €/kWh, the qualification is conditioned by the level of charge capacity cost and charge efficiency. In the case of having a midrange discharge efficiency ($\eta_d = 50\%$), the energy capacity cost qualification criterion is shifted leftwards towards border (b) that omits configurations with $\hat{c} \geq 20$ €/kWh. However, this limit is conditioned by having perfect remaining parameters, meaning that both the charge efficiency (η_c) is high (95%) and the charge capacity cost (c_c) and discharge capacity cost (c_d) are very low (35 €/kW). This can be eluded by reducing the energy capacity cost to $\hat{c} < 5$ €/kWh to reach the unconditioned region. At a low discharge efficiency ($\eta_d = 25\%$), the energy capacity cost requirement (c) is even more stringent, resulting in the exclusion of all configurations with an energy capacity cost (\hat{c}) of 5 €/kWh or greater. A very low energy capacity cost may compensate for the low discharge efficiency, but this is also conditioned by a low charge capacity cost (c_c) and a charge efficiency of at least 50%. These conditions suggest that low-efficiency storage technologies may be viable options, provided they come at an exceedingly low cost.

The depicted borders of the design space, derived from cost optimization, can serve as optimal design approaches for novel storage technologies. Specifically, the three borders can signify three optimal design strategies that storage developers should pursue. The energy capacity cost and discharge efficiency for the emerging technologies listed in Table I are also shown in Fig. 9, alongside the optimization results. Among the emerging storage technologies, ACAES and LAES are found to be situated near design strategy (a) based on their combination of energy capacity cost and discharge efficiency. The remainder is located near design strategy (b) or (c). The RFB technology is absent from the graph as its corresponding energy capacity cost ($\hat{c} = 115$ €/kWh) falls beyond the limit of the sample space considered in this study. We find that none of the candidates meet the unconditioned qualification

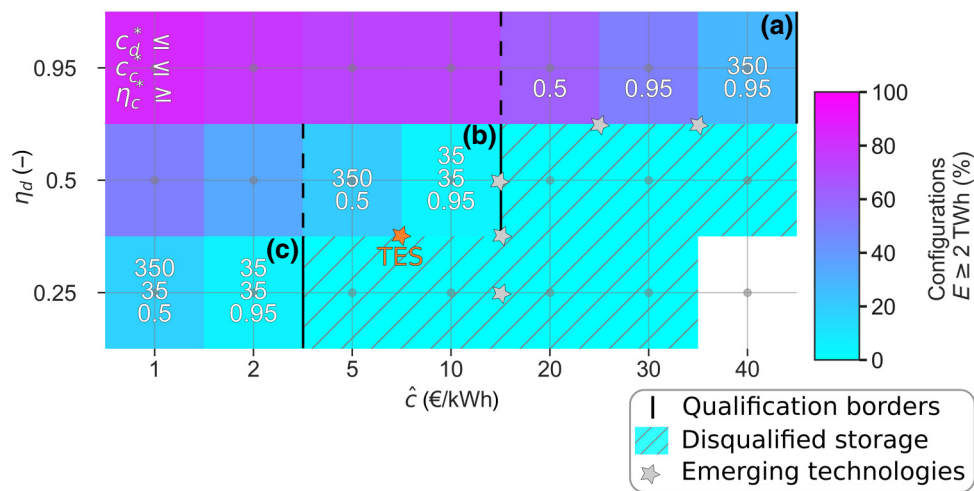


FIG. 9. Cost and efficiency requirements for the fully sector-coupled system. Share of configurations from the sample space (indicated by color) fulfilling $E \geq 2$ TWh at combinations of energy capacity costs (primary axis) and discharge efficiencies (secondary axis). The hatched area indicates combinations at which no configuration entails energy capacity $E \geq 2$ TWh. The white annotations are additional conditions that need to be met for the considered combination to qualify. If no annotation is present, the combination is not conditioned by additional parameter requirements. The border at which the storage only just qualifies is indicated for each discharge efficiency level. This is done for conditioned (solid lines) and unconditioned (dashed lines) qualifications. The lines also delineate three design strategies (a)–(c). The attributes of the emerging technologies in Table I are indicated with stars. Because of the discreteness and the multidimensionality of the parameter space, the emerging technology indicators are located in between the investigated cells, unless they exactly match. See Fig. S8 within the Supplemental Material [56] for combinations of the power capacity costs (c_c and c_d) and the efficiencies (η_c and η_d).

criteria solely based on their energy capacity cost and discharge efficiency. To qualify for the conditioned region, the storage needs, on top of having either high discharge efficiency or low energy capacity cost, additional well-performing attributes. The TES technology benefits from not only having the lowest energy capacity cost but also the lowest charge capacity cost ($c_c = 38$ €/kW) concurrent with a high charge efficiency ($\eta_c = 98\%$), which makes it a promising configuration. Based on its location in the chart, it still needs either a higher discharge efficiency or lower energy capacity cost to clearly qualify. Because of its low discharge efficiency and concurrent midrange energy capacity cost, PTES follows a mixed design strategy between (b) and (c) that positions it in the disqualified region. The two design strategy-(a) technologies, ACAES and LAES, have the highest discharge efficiencies ($\eta_d = 65\%$). This is still 30 percentage points lower than the considered discharge efficiency in (a). Since a large variation in optimal energy capacity deployment is explained by the discharge efficiency (Table VI), this reduces its chance to qualify. To test these hypotheses, we evaluate the energy capacity deployment with the exact parameters for the candidates in Table I, which leads to the same conclusion (Fig. 10) that only TES shows a noticeable deployment, mainly due to its low energy capacity cost and low charge power capacity cost. It does, however, not entail the optimal energy capacity sufficient to qualify for the design space.

D. Storage-X impact on the energy system design

Every system composition and all storage integration scenarios have been obtained for a CO₂ emissions constraint of 5%. This involves a large roll-out of non-carbon-emitting generation technologies. Across all storage scenarios, the electricity generation is on average supplied by 56% wind, 34% solar, and 6% hydropower. The remaining 4% is covered with fossil-fueled power plants, biomass CHP, or nuclear (see Fig. S9 within the Supplemental Material [56]). The mix of backup reserves and storage (excluding PHS) is a result of the optimization and is impacted by the deployment of storage-X (top plot in Fig. 11). At low levels of storage-X penetration, based on the deployed energy capacity, a high share of flexible generation is needed, mainly provided by gas-powered OCGT and CHP (supplying both heat and power), both showing low load hours equivalent to 8.3% and 3.3% utilization rates throughout a full year. In comparison, in SC1, fossil-fueled generation can be deployed with a much higher utilization rate: 43.4% for CCGT (see Fig. S10 in Supplemental Material [56]). Increasing the storage-X deployment reduces these capacities noticeably. CHP fueled with biomass is weakly affected since the model finds it optimal to utilize the full potential of biomass across all scenarios.

Battery capacity is replaced as storage-X increases its load coverage, indicated by the linear decay of battery discharge capacity (bottom plot in Fig. 11). For

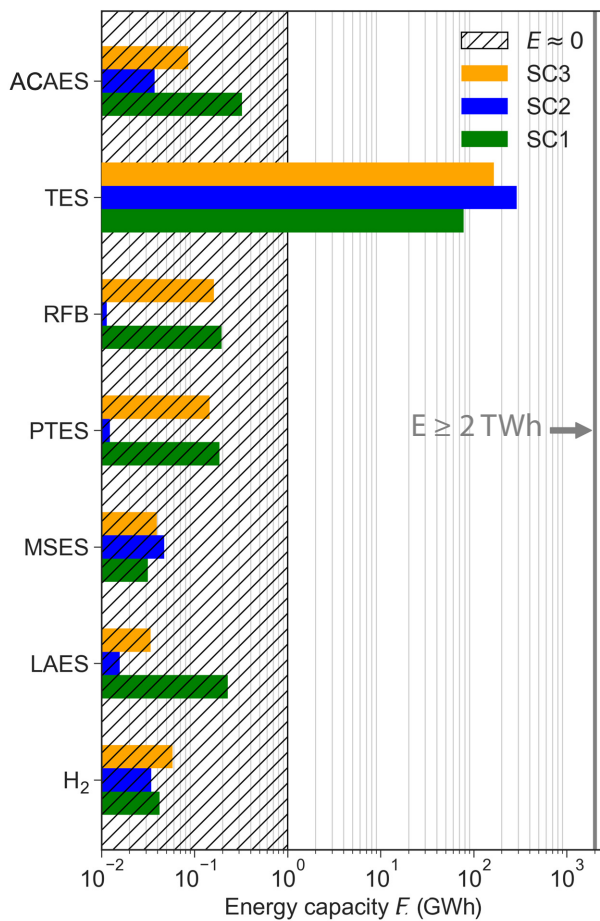


FIG. 10. Optimal energy capacity of storage-X candidates. Comparison of the energy capacity deployment if the technology listed in Table I was made available in PyPSA-Eur-Sec. Because of its low energy capacity cost and charge power capacity cost, TES is the only storage technology that entails a noticeable storage deployment on a European scale (100–300 GWh), but does not qualify for the imposed threshold of ≥ 2 TWh. The rest of the candidates entail a negligible energy capacity (< 1 GWh).

comparison, the discharge capacity of storage-X is also depicted to indicate that the battery capacity deployment is linearly dependent on the storage-X load coverage, but does not show the same proportionality with storage-X discharge capacity. This is due to the fact that load coverage is also determined by other storage-X attributes. While storage-X is capable of replacing battery capacities with increasing load coverage, it does not adapt the temporal short-term characteristics since most of the storage-X configurations result in a duration (i.e., energy-to-power ratio) of approximately 50 h (see Fig. S11 within the Supplemental Material [56]). The maximum duration within the configurations equals 190.3 h, equivalent to 7.6 days. Concurrently, most batteries show durations of 3 or 6 h (see Fig. S12 within the Supplemental Material [56]).

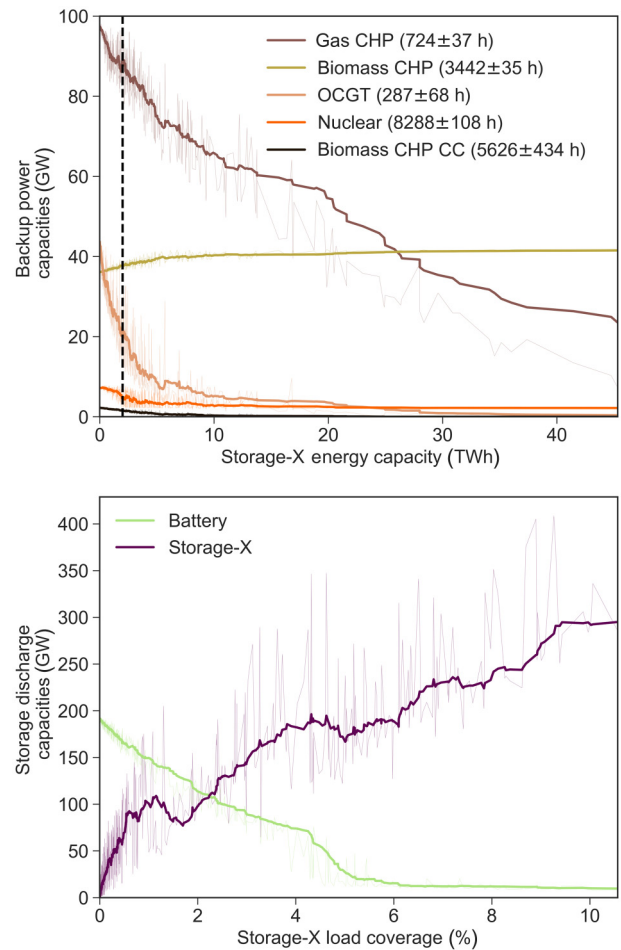


FIG. 11. Backup power and storage discharge capacity. Top: power capacities of dispatchable thermal power plants for the 724 storage samples sorted by the storage-X energy capacity. Numbers in parentheses indicate the average full load hours \pm the root-mean-square deviation of all storage scenarios. The vertical dashed line indicates the ≥ 2 TWh threshold imposed to derive the design space. Bottom: storage discharge power capacities sorted by the storage-X load coverage. Thick lines show the moving average of the 15 previous configurations. Gas power plants (CHP and OCGT) and battery capacity drop continuously as storage-X is deployed. For the results of SC1 and SC2, see Fig. S10 within the Supplemental Material [56].

Another alternative to new storage facilities is deploying excess capacity of renewable generators, which entails a less energy-efficient system as more energy is curtailed instead of being utilized. Whether this entails a more expensive system is evaluated in Fig. 12. Here, the normalized system cost (i.e., 1 corresponds to the most expensive system in which storage-X is not deployed) is acquired for each storage configuration and compared with the level of renewable curtailment [Eq. (2)]. In general, a low curtailment is observed ($< 3\%$ for all configurations). Some observations can, however, be made.

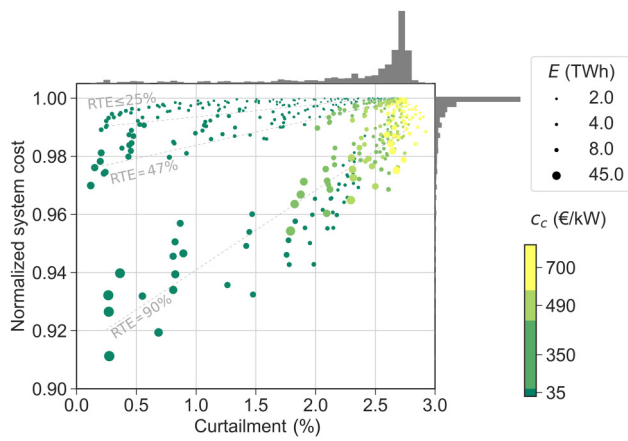


FIG. 12. System cost reduction and renewable curtailment. Normalized system cost (secondary axis) ordered by the level of renewable curtailment (primary axis) for the 724 storage samples. The scatters are colored according to the corresponding charge capacity cost (c_c) and are furthermore sized according to the optimal energy capacity. The results are obtained with the fully sector-coupled system (SC3). See Fig. S13 within the Supplemental Material [56] for the same depictions of SC1 and SC2.

All configurations with a high charge capacity cost are concentrated within the same upper level of renewable curtailment. Thus, expensive charge components can be associated with more curtailment. As the charge capacity cost is reduced, the system encounters lower levels of renewable curtailment. Concurrently, the system cost reduction potential is improved. The best storage-X configuration reduces the total system cost by 9%.

Additionally, the level of system cost reduction is shown to depend on the round-trip efficiency ($\text{RTE} = \eta_c \eta_d$). Two distinct groups of scenarios form (an artifact of the parameter discreteness): one group containing midlow RTE ($\leq 47\%$) configurations and another one with the high RTE (90%). A high RTE is a prerequisite to obtaining the steepest reduction proportional to the curtailment reduction. A high RTE is, however, not a guarantee for obtaining the lowest system cost. For example, low charge capacity cost configurations with midrange RTE are capable of achieving a lower system cost than expensive charge capacity with high RTE. Equivalently, low curtailment is not a guarantee for low system cost either since it depends on the portfolio of storage technologies. Thus, obtaining a highly energy-efficient system, in terms of low energy curtailment, is not necessarily the cost-optimal strategy.

For the other two system compositions, curtailment of renewable energy is higher, with less than 7% in SC1 and less than 4% in SC2 (see Fig. S13 within the Supplemental Material [56]). The variation in curtailment between the three system compositions can be explained by the flexible demand that arises from sector coupling. In particular, the large-scale hydrogen production in SC3 results in a higher

utilization rate of renewable energy, as it can be produced at any time, independently of the concurrent demand, provided that hydrogen storage or transport is available. For SC1 and SC2, the largest reductions in system cost are 12% and 9%, respectively, at the best storage-X configuration. When considering 95% of the configurations (i.e., the 95th percentile), the largest system cost reductions decrease to 6%, 4%, and 4% for SC1, SC2, and SC3, respectively.

V. DISCUSSION

This study aims to find the requirements for an additional electricity storage technology, storage-X, to be deployed in the cost-optimal sector-coupled energy system. In the following, we discuss our findings and the corresponding implications.

First, our results support the findings of Refs. [14,31–33] that the discharge efficiency and storage energy capacity cost are the parameters that potentially, if improved, entail the highest rise in storage deployment. The significance of the discharge efficiency can to some extent be explained by the serial connection of the storage-X components of which the discharge stage is the last element. As an example, we imagine the case in which the discharge efficiency is worsened, while the other input parameters are fixed. In that case, to ensure the same storage electricity output, the storage energy capacity and power capacity for charging have to be enlarged. This requires higher investments in both of the components. As a comparison, the capacity cost in general (charge, storage, discharge) does not have such a serial-accumulating impact, but only alters the investments in the considered component. The energy capacity cost is linked to the cost-optimal size of the storage, which is why such high sensitivity is observed in the optimal energy capacity deployment to this parameter. As large energy capacity allows balancing low-frequency droughts where batteries are a very expensive option, this makes it a parameter of high importance.

Here, we also highlight the importance of a third parameter: the charge capacity cost. Renewable curtailment is related to the cost of charging (Fig. 12). The system can either deploy, if cost optimal, sufficient charge capacity to utilize the full renewable potential, or, lacking storage charge capacity, curtail some of it. Thus, it is a trade-off between investments in larger charge capacity or more renewable curtailment, which can explain the significance of this input parameter. This was not shown in prior literature [31] inspecting the parameter importance of electricity storage. A share of the discrepancy can be related to the distinct assumptions concerning electricity transmission. Using a copperplate model, i.e., ignoring electricity transmission constraints over large regions, can lead to a misestimation of the renewable electricity generation [74]. This also implies misestimating the renewable curtailment

and, consequently, underestimating the importance of the storage charge capacity cost.

Second, our study identifies the trade-offs between cost and efficiency. A storage with high discharge efficiency and very low energy capacity cost would have the best chances of being competitive. If this is not attainable, a trade-off between cost and efficiency arises, i.e., a high cost can be compensated by a high efficiency. Our results show that the energy capacity cost requirement is driven by the attainable discharge efficiency, and vice versa. Here, we have identified three design strategies for storage to play a prominent role in future renewable energy systems. The optimal design strategies are to select either

- (a) high discharge efficiency ($\eta_d \geq 95\%$);
- (b) midrange discharge efficiency ($\eta_d \geq 50\%$) if the energy capacity cost $\hat{c} \leq 10$ €/kWh; or
- (c) low discharge efficiency ($\eta_d \leq 25\%$) if the energy capacity cost $\hat{c} \leq 2$ €/kWh.

None of the emerging technologies fulfills these requirements. Flow-redox batteries are discarded due to their high energy capacity cost. The remainders are not good enough in any of the (a), (b), or (c) design strategies. The only exception is TES, which is attributed with the lowest-energy capacity cost of all candidates. For this reason, as the only candidate, it shows a noticeable optimal storage deployment. However, to fully qualify for design strategy (b) (and increase its optimal deployment by one order of magnitude), it would need to alter its discharge efficiency from 38% to 50%. This might not be attainable with the applied discharge technology (Brayton cycle), depending on the available temperature ratio. In that case, it needs to reduce its energy capacity cost from 8 to < 5 €/kWh. Another technology, PTES, is discarded due to not complying with the optimal trade-off. It has the combination of low discharge efficiency [design strategy (c)] and midrange energy capacity cost [design strategy (b)]. Thus, our results also show that it is optimal to pursue one of these design strategies, while hybrid strategies have both low potentials and can be difficult to realize.

In the remainder of this section, we discuss the limitations of this study.

Applying the chosen temporal resolution with 3-hourly time steps implies that the variation within these time steps is perfectly balanced without any cost. For this reason, this framework does not cover nor calculate the potential for storage used for such short-term purposes. In addition to this, with the applied 37-node network resolution, we do not include bottlenecks in the transmission connecting different regions within the countries but only account for the cross-border transmission. A higher storage capacity would be expected to account for such additional transmission constraints in a more detailed network representation.

We do not allow grid services from BEV batteries. Since this assumption mainly determines the volume of stationary battery storage, it is a question of whether storage should be located in the low-voltage grid provided by BEV batteries or provided at the high-voltage level by utility-scale battery storage. In this model framework, batteries are primarily used to smoothen the diurnal fluctuation in solar generation. At a certain level of storage-X penetration, we do see that the stationary batteries are replaced by storage-X. For this reason, and due to the competition between V2G and batteries, the inclusion of V2G would also impose an upper limit on the storage-X deployment. Another assumption is related to the inclusion of hydrogen (H_2). The hydrogen bus in our model does not have a direct link to the electricity bus (i.e., fuel cells or H_2 -fired gas power plants are excluded). This assumption offsets some flexibility that would have been contained by the additional usage option of the H_2 carrier.

As we investigate flexibility options and suggest gas power plants as new backup capacities, this is established on cost assumptions that do not reflect the recent development of commodity prices of, e.g., gas. We perform an overnight optimization that does not correspond to a specific year but is to resemble a possible near-future system prior to full decarbonization. In the system today, a large number of central fossil-fueled power plants are still either active or kept on standby. Thus, some of these flexibility options might still be valuable assets in commission that the backup capacity in our study could also represent.

As this is an overnight optimization, we do not consider the transition toward the final system. The electricity generation capacity (including fossil-fueled and renewable generators) and the storage capacity are co-optimized concurrently. From the literature, we have seen large storage quantities only at the late stage of the renewable penetration. For this reason, a transitional optimization would entail the renewables to be rolled out, eventually reaching a certain level at which storage would be added to the system. In that sense, the storage ensemble does not influence the share of generation sources, which is the case in this study. In pathway optimization, there is also the option of learning. The considered portfolio of storage candidates has differences within modularity and technological simplicity and is expected to gain differently from scale-up. A pathway optimization with endogenous learning would shed light on this and could make the differences in the potential of the different storage candidates even more pronounced.

In this study, we evaluate the integration of single configurations of storage-X in parallel scenarios. Multiple storage-X do not appear simultaneously in the same scenario. Therefore, the modeled competition is only related to existing storage technologies (stationary Li-ion battery storage) and other flexibility options (backup power plants and demand-side management) in the system, and it does

not account for the potential competition between multiple storage-X technologies. Such competition would better represent reality and it could furthermore shed light on potential alliances of storage that in combination could be more beneficial for the system than one unique dominant option. Future work should address this.

VI. CONCLUSION

To explore the requirements of a successful additional storage technology, storage-X, we attained a design space established on 724 storage samples to identify the configurations that would lead to substantial storage deployment (here, equivalent to ≥ 2 -TWh energy capacity) in a highly renewable sector-coupled energy system. This was performed when accounting for the competition with stationary battery storage, flexible generation technologies, and possible demand-side management.

We find that energy capacity cost and discharge efficiency are the parameters leading to the highest impact on the optimal storage-X deployment. Energy capacity cost is linked to the ability to provide low-frequency balancing of renewable droughts, and the importance of discharge efficiency is related to the serial dependence of the storage components. On top of this, the charge capacity cost shows high relative importance as well, here explained by its noticeable impact on the level of renewable curtailment.

For a cost-optimal deployment, an additional electricity storage technology is required to have (a) discharge efficiency of at least 95%, (b) discharge efficiency of at least 50% in combination with a low energy capacity cost (10 €/kWh), or (c) a very low energy capacity cost (2 €/kWh) if the discharge efficiency is 25%. Comparing our findings with seven emerging technologies reveals that none of them fulfills these requirements. The only noticeable deployment is observed for TES, which is a candidate for design strategy (b), but to fully qualify, it needs to increase its discharge efficiency from 38% to 50% or reduce its energy capacity cost from 8 to < 5 €/kWh.

Finally, we assessed the system impact of the integration of storage-X. Our analysis shows that the integration of an additional storage technology can lead to a system cost reduction of up to 9%, but only if the technology has a high round-trip efficiency (RTE $\geq 90\%$) and a low charge capacity cost ($c_c = 35$ €/kW).

ACKNOWLEDGMENTS

E.K.G., M.V., and G.B.A. are partially or fully funded by the GridScale project supported by the Danish Energy Technology Development and Demonstration Program under Grant No. 64020-2120. We are thankful for helpful comments from Fredrik Hedenus, Lina Rechenberg, Martin Greiner, Stefan Lechner, and Sleiman Farah.

APPENDIX A: DISAGGREGATION OF REPORTED STORAGE TECHNOLOGY COST ASSUMPTIONS

This appendix describes the procedure of converting reported data on emerging storage technologies to fit the representation of storage-X in this paper, with the results presented in Table I.

In some of the considered technology cost reviews, reported power capacity costs cover expenses related to both charging and discharging. It is given by the aggregate power capacity cost C_P , accompanied by a power capacity cost ratio r_C . To disaggregate C_P into charge and discharge power capacity costs, c_c and c_d , we define the two equations

$$C_P = \frac{1}{\eta_{RT}} c_c + c_d, \quad r_C = \frac{c_c}{c_d}, \quad (\text{A1})$$

where η_{RT} is the round-trip efficiency acquired from the literature. From the two above equations, the charge and discharge capacity costs can be explicitly determined:

$$c_c = r_C c_d, \quad c_d = C_P - \frac{1}{\eta_{RT}} c_c. \quad (\text{A2})$$

Along with the ratio r_η between the charge and discharge efficiencies, η_c and η_d , we define the two equations

$$\eta_{RT} = \eta_c \eta_d, \quad r_\eta = \frac{\eta_c}{\eta_d}. \quad (\text{A3})$$

The round-trip efficiency is then split into the charge and discharge efficiencies:

$$\eta_c = r_\eta \eta_d, \quad \eta_d = \frac{\eta_{RT}}{\eta_c}. \quad (\text{A4})$$

Standing loss is reported as a percentage, given as an energy loss per day relative to the energy content of the previous day. The state of charge is assumed to follow an exponential decay. The percentage can be converted into a time constant, which represents the time passed before the storage reaches a substantially low state of charge (here, 36.8%). We call this time constant the self-discharge time τ_{SD} , and it is determined by the equation [Eq. (1)]

$$\tau_{SD} = -\ln(1 - \Delta \bar{e}_{\text{loss}})^{-1}, \quad (\text{A5})$$

where $\Delta \bar{e}_{\text{loss}} = \bar{e}_t - \bar{e}_{t-1}$ is the relative daily energy loss that in the reporting is assumed to be constant.

APPENDIX B: PYPSA-EUR-SEC

The system is modeled using the open energy system model PyPSA-Eur-Sec [29]. The dispatch and capacity of generators, storage units, and conversion links in each

node are optimized such that the total system cost is minimized, which is mathematically written as

$$\min_{G_{n,s}, E_{n,s}, F_l, g_{n,s,t}} \left[\sum_{n,s} c_{n,s} G_{n,s} + \sum_{n,s} \hat{c}_{n,s} E_{n,s} + \sum_l c_l F_l + \sum_{n,s,t} o_{n,s,t} g_{n,s,t} \right], \quad (\text{B1})$$

where $c_{n,s}$ and $\hat{c}_{n,s}$ are the annualized costs for generator and storage power capacity $G_{n,s}$ and storage energy capacity $E_{n,s}$ for technology s in node n ; c_l is the fixed annualized cost for capacity F_l of link l ; $o_{n,s,t}$ is the marginal cost of generation and storage dispatch $g_{n,s,t}$ at time t .

The optimization is subject to a list of linear equality and inequality constraints, of which two of them are

$$\sum_s g_{n,s,t} + \sum_l \alpha_{n,l,t} f_{l,t} = d_{n,t} \leftrightarrow \lambda_{n,t} \quad \text{for all } n, t, \quad (\text{B2})$$

$$\sum_{n,s,t} \varepsilon_s \frac{g_{n,s,t}}{\eta_{n,s}} \leq \text{CAP}_{\text{CO}_2} \leftrightarrow \mu_{n,t} \quad \text{for all } n, t. \quad (\text{B3})$$

Equation (B2) is an equality constraint that ensures that the energy generation $g_{n,s,t}$, dispatch or charging of storage and energy imports or exports $f_{l,t}$ are exactly balanced with the demand $d_{n,t}$ in all nodes n at all times t . Here, $f_{l,t}$ is the power flow through link l at time t , and $\alpha_{n,l,t}$ includes the direction and efficiency of the flow in the links. The equality constraint entails a Lagrange multiplier $\lambda_{n,t}$ that is the shadow price of the energy carrier.

Equation (B3) is an inequality constraint that enforces an upper bound on the total annual CO₂ emissions in the system (i.e., a global CO₂ emission constraint) that is given as a percentage of the 1990-emission level. Here, ε_s is the CO₂ intensity in tonne-CO₂ per MWh_{th}, and $\eta_{n,s}$ is the efficiency. The PyPSA-Eur-Sec model is capable of tracing direct emissions from power generation, energy conversion, and industrial processes. It can furthermore deploy negative-emission technologies (direct air capture or carbon capture on point sources such as thermal power plants) if cost optimal. The calculations do not include life-cycle emissions on each of the technologies. The inequality constraint entails a Lagrange multiplier $\mu_{n,t}$ that is the CO₂ shadow price.

The history of charging and discharging in combination with the level of standing loss determines the state of charge of the storage at any time t . The state of charge is constrained to not exceed the storage energy capacity. Here, the energy content $e_{n,s,t}$ of an energy storage technology s in node n at time t is given by the following energy balance, when accounting for standing loss (η_0) and efficiency losses (η_c and η_d) and given the energy content at

the previous time t :

$$e_{n,s,t} = \eta_0 e_{n,s,t-1} + \eta_c |\Delta e_{n,t}^+| - \eta_d |\Delta e_{n,t}^-|, \\ 0 \geq e_{n,s,t} \geq E_{n,s}. \quad (\text{B4})$$

Here, $|\Delta e_{n,t}^+|$ is the absolute electricity stored and $|\Delta e_{n,t}^-|$ is the dispatched electricity in node n at time t . The standing loss is in this equation represented by an efficiency η_0 that equals 1 in the case $\tau_{\text{SD}} = \text{inf}$. The energy content cannot exceed the storage energy capacity, i.e., $e_{n,s,t} \leq E_{n,s}$.

All technology investment capacity costs are annualized assuming a lifetime of each asset and a discount rate r of 7%:

$$c_{n,s} = c_{n,s}^{\text{inv}} \frac{r(1+r)^n}{(1+r)^n - 1} \quad (\text{B5})$$

with $c_{n,s}$ the annualized costs and $c_{n,s}^{\text{inv}}$ the capacity costs.

APPENDIX C: REDUCTION OF THE SAMPLE SPACE BASED ON FILTER M

To reduce computation time, when repeating the calculations for the same sample space Q in the three system compositions, we introduce a filtering metric M [Eq. (C1)]. The M metric represents the ratio between the capacity costs and the efficiencies. If the ratio exceeds a threshold, the storage becomes noncompetitive and will, for this reason, most probably not be part of the optimal design space. The threshold is derived from the optimization results obtained with SC1. We compute the ratio of capacity cost and efficiency as

$$M = \frac{(c_c/\lambda_1)(c_d/\lambda_2) + \hat{c}}{\eta_c \eta_d} \leq \max\{M(E = 2 \text{ TWh})\}. \quad (\text{C1})$$

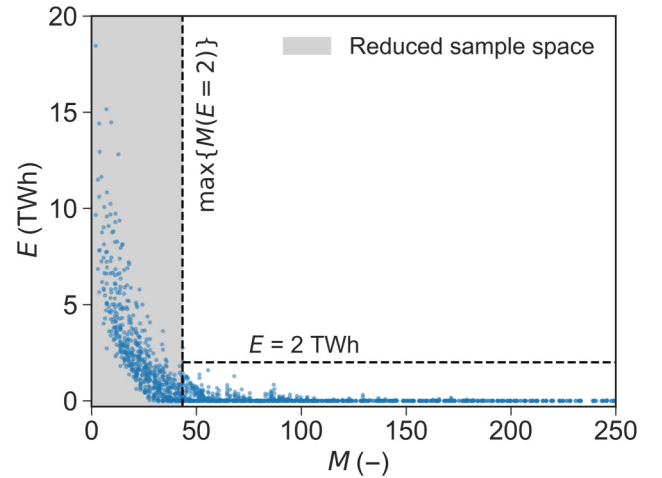


FIG. 13. Reduction of the sample space. Reduction based on M defined in Eq. (C1) obtained with results for the electricity system.

Here, λ_1 and λ_2 are scaling factors obtained by fitting Eq. (C1) to the output (E) in SC1. By matching the size of the design space [$Q(E \geq 2 \text{ TWh})$] and the number of configurations that meet the condition in Eq. (C1), the scaling factors $\lambda_1 = 57$ and $\lambda_2 = 175$. The obtained reduction of the sample space is illustrated in Fig. 13. The sample space Q containing 2016 configurations is reduced to 593 configurations. Subsequently, to retain the exterior of the considered sample space (combinations in which upper parameter limits are included), 131 additional configurations are included, entailing a final sample space of 724 configurations.

-
- [1] UN: Paris agreement (2015), https://sustainabledevelopment.un.org/content/documents/17853paris_agreement.pdf.
- [2] M. Victoria, E. Zeyen, and T. Brown, Speed of technological transformations required in Europe to achieve different climate goals, *Joule* **6**, 1066 (2022).
- [3] F. Ueckerdt, R. Brecha, and G. Luderer, Analyzing major challenges of wind and solar variability in power systems, *Renewable Energy* **81**, 1 (2015).
- [4] K. Engeland, M. Borga, J.-D. Creutin, B. François, M.-H. Ramos, and J.-P. Vidal, Space-time variability of climate variables and intermittent renewable electricity production—A review, *Renewable Sustainable Energy Rev.* **79**, 600 (2017).
- [5] E. Bianchi, E. Guozden, and R. Kozulj, Assessing low frequency variations in solar and wind power and their climatic teleconnections, *Renewable Energy* **190**, 560 (2022).
- [6] H.-K. Ringkjøb, P. M. Haugan, P. Seljom, A. Lind, F. Wagner, and S. Mesfun, Short-term solar and wind variability in long-term energy system models—A European case study, *Energy* **209**, 118377 (2020).
- [7] D. Schindler, H. D. Behr, and C. Jung, On the spatiotemporal variability and potential of complementarity of wind and solar resources, *Energy Convers. Manage.* **218**, 113016 (2020).
- [8] M. Victoria, K. Zhu, T. Brown, G. B. Andresen, and M. Greiner, The role of photovoltaics in a sustainable European energy system under variable CO₂ emissions targets, transmission capacities, and costs assumptions, *Prog. Photovoltaics: Res. Appl.* **28**, 483 (2020).
- [9] I. Graabak and M. Korpaas, Variability characteristics of European wind and solar power resources—A review, *Energies* **9**, 449 (2016).
- [10] J. Kapica, F. Canales, and J. Jurasz, Global atlas of solar and wind resources temporal complementarity, *Energy Convers. Manage.* **246**, 114692 (2021).
- [11] D. Heide, L. von Bremen, M. Greiner, C. Hoffmann, M. Speckmann, and S. Bofinger, Seasonal optimal mix of wind and solar power in a future, highly renewable Europe, *Renewable Energy* **35**, 2483 (2010).
- [12] P. Tapetado, M. Victoria, M. Greiner, and J. Usaola, Exploring backup requirements to complement wind, solar and hydro generation in a highly renewable Spanish power system, *Energy Strategy Rev.* **38**, 100729 (2021).
- [13] A. Aktaş, in *Advances in Clean Energy Technologies*, edited by A. K. Azad (Academic Press, 2021), p. 377.
- [14] F. Tong, M. Yuan, N. S. Lewis, S. J. Davis, and K. Caldeira, Effects of deep reductions in energy storage costs on highly reliable wind and solar electricity systems, *iScience* **23**, 101484 (2020).
- [15] M. Victoria, K. Zhu, T. Brown, G. B. Andresen, and M. Greiner, The role of storage technologies throughout the decarbonisation of the sector-coupled European energy system, *Energy Convers. Manage.* **201**, 111977 (2019).
- [16] C. Cheng, A. Blakers, M. Stocks, and B. Lu, Pumped hydro energy storage and 100 renewable electricity for East Asia, *Global Energy Interconnection* **2**, 386 (2019).
- [17] C. Andrey, P. Barberi, L. Nuffel, *et al.*, European Commission, Directorate-General for Energy, *Study on Energy Storage: Contribution to the Security of the Electricity Supply in Europe* (Publications Office, 2020), <https://data.europa.eu/doi/10.2833/077257>.
- [18] IHA: Hydropower status report 2021 (2021), <https://www.hydropower.org/publications/2021-hydropower-status-report>.
- [19] F. Geth, T. Brijs, J. Kathan, J. Driesen, and R. Belmans, An overview of large-scale stationary electricity storage plants in Europe: Current status and new developments, *Renewable Sustainable Energy Rev.* **52**, 1212 (2015).
- [20] D. Choi, N. Shamim, A. Crawford, Q. Huang, C. K. Vartanian, V. V. Viswanathan, M. D. Paiss, M. J. E. Alam, D. M. Reed, and V. L. Sprenkle, Li-ion battery technology for grid application, *J. Power Sources* **511**, 230419 (2021).
- [21] SolarPower Europe: European market outlook for residential battery storage 2022–2026 (2022), https://api.solarpowereurope.org/uploads/European_Market_Outlook_BEI_SS_SPE_2022_d27fb18f8e.pdf.
- [22] O. Schmidt, S. Melchior, A. Hawkes, and I. Staffell, Projecting the future levelized cost of electricity storage technologies, *Joule* **3**, 81 (2019).
- [23] G. Glenk, R. Meier, and S. Reichelstein, Cost dynamics of clean energy technologies, *Schmalenbach J. Bus. Res.* **73**, 179 (2021).
- [24] Y. Scholz, H. C. Gilsa, and R. C. Pietzcke, Application of a high-detail energy system model to derive power sector characteristics at high wind and solar shares, *Energy Econ.* **64**, 568 (2017).
- [25] F. Cebulla, T. Naegler, and M. Pohl, Electrical energy storage in highly renewable European energy systems: Capacity requirements, spatial distribution, and storage dispatch, *J. Energy Storage* **14**, 211 (2017).
- [26] H. C. Gils, H. Gardian, and J. Schmutge, Interaction of hydrogen infrastructures with other sector coupling options towards a zero-emission energy system in Germany, *Renewable Energy* **180**, 140 (2021).
- [27] F. Neumann, E. Zeyen, M. Victoria, and T. Brown, Benefits of a hydrogen network in Europe, Available at SSRN: <https://ssrn.com/abstract=4173442> (2022).
- [28] C. A. Hunter, M. M. Penev, E. P. Reznicek, J. Eichman, N. Rustagi, and S. F. Baldwin, Techno-economic analysis of long-duration energy storage and flexible power generation technologies to support high-variable renewable energy grids, *Joule* **5**, 2077 (2021).

- [29] T. Brown, D. Schlachtberger, A. Kies, S. Schramm, and M. Greiner, Synergies of sector coupling and transmission reinforcement in a cost-optimised, highly renewable European energy system, *Energy* **160**, 720 (2018).
- [30] S. Wang, B. Tarroja, L. S. Schell, and S. Samuelsen, Determining cost-optimal approaches for managing excess renewable electricity in decarbonized electricity systems, *Renewable Energy* **178**, 1187 (2021).
- [31] N. A. Sepulveda, J. D. Jenkins, A. Edington, D. S. Malapragada, and R. K. Lester, The design space for long-duration energy storage in decarbonized power systems, *Nat. Energy* **6**, 506 (2021).
- [32] J. A. Dowling, K. Z. Rinaldi, T. H. Ruggles, S. J. Davis, M. Yuan, F. Tong, N. S. Lewis, and K. Caldeira, Role of long-duration energy storage in variable renewable electricity systems, *Joule* **4**, 1907 (2020).
- [33] M. Ziegler, J. M. Mueller, G. D. Pereira, J. Song, M. Ferrara, Y. Chiang, and J. E. Trancik, Storage requirements and costs of shaping renewable energy toward grid decarbonization, *Joule* **3**, 2134 (2019).
- [34] W.-P. Schill, Electricity storage and the renewable energy transition, *Joule* **4**, 2059 (2020).
- [35] M. Parzen, F. Neumann, A. H. Van Der Weijde, D. Friedrich, and K. Aristides, Beyond cost reduction: Improving the value of energy storage in electricity systems, *Carbon Neutrality* **1**, 26 (2022).
- [36] H. Lund, P. A. Østergaard, D. Connolly, I. Ridjan, B. V. Mathiesen, F. Hvelplund, J. Z. Thellufsen, and P. Sorknæs, Energy storage and smart energy systems, *Int. J. Sustainable Energy Plan. Manage.* **11**, 3 (2016).
- [37] <https://github.com/ebbekyhl/storageX.git>.
- [38] K. R. Gautam, G. B. Andresen, and M. Victoria, Review and techno-economic analysis of emerging thermo-mechanical energy storage technologies, *Energies* **15**, 00 (2022).
- [39] Danish Energy Agency: Technology data for renewable fuels (2022), https://ens.dk/sites/ens.dk/files/Analyser/technology_data_for_renewable_fuels.pdf.
- [40] Danish Energy Agency: Technology data for generation of electricity and district heating (2022), https://ens.dk/sites/ens.dk/files/Analyser/technology_data_catalogue_for_el_and_dh.pdf.
- [41] C. Budischak, D. Sewell, H. Thomson, L. Mach, D. E. Veron, and W. Kempton, Cost-minimized combinations of wind power, solar power and electrochemical storage, powering the grid up to 99.9, *J. Power Sources* **225**, 60 (2013).
- [42] Power Technology: Kraftwerk Huntorf—Compressed air energy storage system, Germany (2022), <https://www.power-technology.com/marketdata/kraftwerk-huntorf-compressed-air-energy-storage-system-germany/>.
- [43] Power Technology: McIntosh power plant—Compressed air energy storage system, US (2022), <https://www.power-technology.com/marketdata/mcintosh-power-plant-compressed-air-energy-storage-system-us/>.
- [44] NEW ATLAS: China turns on the world's largest compressed air energy storage plant (2022), <https://newatlas.com/energy/china-100mw-compressed-air/>.
- [45] E. Barbour and D. L. Pottie, Adiabatic compressed air energy storage technology, *Joule* **5**, 1914 (2021).
- [46] J. H. Vinco, A. E. E. da Cunha Domingos, D. C. R. Espinosa, J. A. S. Tenório, and M. dos Passos Galluzzi Baltazar, Unfolding the vanadium redox flow batteries: An in-depth perspective on its components and current operation challenges, *J. Energy Storage* **43**, 103180 (2021).
- [47] J. V. Barreras, S. D. Valdivia Alberti, and M. Schimpe, in *Encyclopedia of Electrical and Electronic Power Engineering* (Elsevier, Oxford, 2023), p. 344.
- [48] P. V. Magazine, China connects world's largest redox flow battery system to grid (2022), <https://www.pv-magazine.com/2022/09/29/china-connects-worlds-largest-redox-flow-battery-system-to-grid/>.
- [49] G. Angelini, A. Lucchini, and G. Manzolini, Comparison of thermocline molten salt storage performances to commercial two-tank configuration, *Energy Proc.* **49**, 694 (2014), proceedings of the SolarPACES 2013 International Conference.
- [50] F. Holy, M. Textor, and S. Lechner, Gas turbine cogeneration concepts for the pressureless discharge of high temperature thermal energy storage units, *J. Energy Storage* **44**, 103283 (2021).
- [51] C. Damak, D. Leducq, H. M. Hoang, D. Negro, and A. Delahaye, Liquid air energy storage (LAES) as a large-scale storage technology for renewable energy integration—A review of investigation studies and near perspectives of LAES, *Int. J. Refrig.* **110**, 208 (2020).
- [52] Power Technology: Greater Manchester Pilsworth liquid air energy storage pre-commercial demonstrator, UK (2022), <https://www.power-technology.com/marketdata/greater-manchester-pilsworth-liquid-air-energy-storage-pre-commercial-demonstrator-uk/>.
- [53] Danish Energy Agency: Technology data for energy storage, update January 2020, Danish Energy Agency and energinet.dk (2020), <https://ens.dk/en/our-services/projections-and-models/technology-data/technology-data-energy-storage>.
- [54] F. Neumann, V. Hagenmeyer, and T. Brown, Assessments of linear power flow and transmission loss approximations in coordinated capacity expansion problems, *Appl. Energy* **314**, 118859 (2022).
- [55] ENTSO-E: Tyndp 2018 (2018), <https://tyndp.entsoe.eu/tyndp2018/>.
- [56] See Supplemental Material at <http://link.aps.org/supplemental/10.1103/PRXEnergy.2.023006> for tables containing the included transmission line capacity and the power generation technology costs, figures showing the temporal balance of electricity supply and demand throughout the optimized year, the sensitivity of storage-X deployment to the weather year and the CO₂ emission constraint, the storage-X configurations qualifying for the design space in all three system compositions, and the impacts on battery and backup capacity deployment, the total system cost, and the renewable curtailment.
- [57] M. Victoria, K. Zhu, E. Zeyen, and T. Brown, Technology-data v0.2.0, <https://github.com/PyPSA/technology-data/tree/v0.2.0> (2020). https://doi.org/10.25832/time_series/2020-10-06.
- [58] Open Power System Data: Data package time series (2020).

- [59] EEA: Corine land cover 2006 (2021), <https://www.eea.europa.eu/data-and-maps/data/clc-2006-raster-4>.
- [60] EEA: Natura 2000 data—The European network of protected sites (2021), <https://www.eea.europa.eu/data-and-maps/data/natura-12>.
- [61] F. Gotzens, H. Heinrichs, J. Hörsch, and F. Hofmann, Performing energy modelling exercises in a transparent way—The issue of data quality in power plant databases, *Energy Strategy Rev.* **23**, 1 (2019).
- [62] F. Hofmann, J. Hampp, F. Neumann, T. Brown, and J. Hörsch, Atlite: A lightweight python package for calculating renewable power potentials and time series, *J. Open Source Softw.* **6**, 3294 (2021).
- [63] H. Hersbach, B. Bell, P. Berrisford, G. Biavati, A. Horányi, J. Muñoz Sabater, J. Nicolas, C. Peubey, R. Radu, I. Rozum, D. Schepers, A. Simmons, C. Soci, D. Dee, and J.-N. Thépaut, ERA5 hourly data on single levels from 1979 to present, Copernicus Climate Change Service (C3S) Climate Data Store (CDS), 2018. <https://doi.org/10.24381/cds.adbb2d47>.
- [64] Danish Energy Agency: Technology data for carbon capture, transport and storage (2021), <https://ens.dk/en/our-services/projections-and-models/technology-data/technology-data-carbon-capture-transport-and>.
- [65] T. T. Pedersen, E. K. Gøtske, D. A. G. B. Andresen, and M. Victoria, Long-term implications of reduced gas imports on the decarbonization of the European energy system, *Joule* **6**, 1566 (2022).
- [66] M. Gimeno-Gutiérrez and R. Lacal-Arántegui, Assessment of the European potential for pumped hydropower energy storage based on two existing reservoirs, *Renewable Energy* **75**, 856 (2015).
- [67] A. Schröder, F. Kunz, J. Meiss, R. Mendeleevitch, and C. von Hirschhausen, Current and prospective costs of electricity generation until 2050, DIW Data Documentation 68, Berlin (2013). <http://hdl.handle.net/10419/80348>.
- [68] M. Ram, D. Bogdanov, A. Aghahosseini, A. Gulagi, A. S. Oyewo, M. Child, U. Caldera, K. Sadovskaia, J. Farfan, L. Barbosa, M. Fasihi, S. Khalili, B. Dalheimer, G. Gruber, T. Traber, F. De Caluwe, H.-J. Fell, and C. Breyer, Global energy system based on 100% renewable energy—Power, heat, transport and desalination sectors. Study by Lappeenranta University of technology and energy watch group, Lappeenranta, Berlin (2019), <https://www.energywatchgroup.org/new-study-global-energy-system-based-100-renewable-energy/>.
- [69] L. Mantzos, N. A. Matei, E. Mulholland, M. Rózsai, M. Tamba, and T. Wiesenthal, JRC-ideas 2015. European Commission, Joint Research Centre (JRC) (2018). <https://doi.org/10.2905/JRC-10110-10001>.
- [70] A. González-Garrido, A. Thingvad, H. Gaztañaga, and M. Marinelli, Full-scale electric vehicles penetration in the Danish island of Bornholm—optimal scheduling and battery degradation under driving constraints, *J. Energy Storage* **23**, 381 (2019).
- [71] M. G. Rasmussen, G. B. Andresen, and M. Greiner, Storage and balancing synergies in a fully or highly renewable pan-European power system, *Energy Policy* **51**, 642 (2012).
- [72] H. Zsiborács, N. H. Baranyai, A. Vincze, L. Zentkó, Z. Birkner, K. Máté, and G. Pintér, Intermittent renewable energy sources: The role of energy storage in the European power system of 2040, *Electronics* **8**, 729 (2019).
- [73] O. Ruhnau and S. Qvist, Storage requirements in a 100% renewable electricity system: Extreme events and inter-annual variability, *Environ. Res. Lett.* **17** 044018, (2021).
- [74] M. Brinkerink, B. Zakeri, D. Huppmann, J. Glynn, B. Ó. Gallachóir, and P. Deane, Assessing global climate change mitigation scenarios from a power system perspective using a novel multi-model framework, *Environ. Model. Softw.* **150**, 105336 (2022).